A holistic approach to assess the exploitation of renewable energy sources for design interventions in the early design phases

Gabriele Lobaccaro[a*], Croce Silvia[b,c], Daniele Vettorato[b], Salvatore Carlucci[d]

[a] *Department of Architecture and Planning, Norwegian University of Science and Technology, Trondheim, Norway.*

[b] *EURAC Research, Institute for Renewable Energy, Bolzano, Italy*

[c] *Department of Civil, Environmental and Architectural Engineering, University of Padova, Padova, Italy*

[d] *Department of Civil and Environmental Engineering, Norwegian University and Science and Technology, Trondheim, Norway.*

Abstract

This study presents a holistic approach applied to assess the exploitation of renewable energy sources for design interventions in the early design phases in a consolidated urban environment. With reference to the cooling season, the approach implies set of environmental analyses focused on twofold assessments: (i) the use of renewable energies sources for active and passive strategies, (ii) the impact on outdoor thermal comfort of the technological solutions and cool materials installed on the buildings' facades. From the definition of the local boundary conditions, preliminary climate analyses were conducted with dynamic simulation tools such as *Ladybug* and *DIVA-for-Rhino*, while numerical and computational fluid dynamics models, such as *ENVI-met* and *OpenFOAM*, were used to carry out microclimate and wind flow analyses. The approach is tested on two existing residential building blocks in a case study district in Bolzano (Italy). The assessment of several design interventions and building technological solutions have been studied: from the (ii) addition of one story volume on the existing buildings, to the (ii) creation of new green areas, and the (iii) installation of building integrated photovoltaic (BIPV), vertical greenery and double skin façade (DSF) systems on the building's façades. The results, divided in practice and policy implications, demonstrate that preliminary analyses play a relevant role to assess the exploitation of renewable energy sources to optimize the use of urban and building surfaces since the early design phases. High-albedo materials on the façades can totally counterbalance the loss of solar potential due to the overshadowing effect of the additional story. The combination of cool materials (e.g., white reflective plaster) and the increment of the buildings' height could reduce about 1°C the thermal discomfort registered during the high thermal peak during the day. Solar and urban airflow analyses allow to optimize the integration of BIPV in a DSF system; while the installation of green façade can reduce the air temperature locally up to about 0.5°C.

Keywords: *Renewable Energy Sources, Design interventions; Solar potential; Urban Airflow; Microclimate;*

Nomenclature

BIPV	building integrated photovoltaic
CFD	computational fluid dynamics
DHW	domestic hot water
DSF	double skin façade
H	mean height of buildings [m]
RH	relative humidity [%]
Irr_{SW}	short-wave radiation [W/m^2]

Irr_{LW}	long-wave radiation [W/m^2]
Irr_{gl}	average annual global solar radiation [kW h/(m^2 a)]
LAI	leaf area index
LAD	leaf area density
MBE	Mean Bias Errors
PET	Physiological Equivalent Temperature
PV	photovoltaic
RES	renewable energy sources
Rel_{err}	Relative error [%]
RMSE	Root Mean Square Errors
ST	solar thermal
T_{air}	air temperature [°C]
T_{mrt}	mean radiant temperature [°C]
T_s	surface temperature [°C]
W	mean width of a street [m]
W_S	wind speed [m/s]

1. Introduction

In the last decades, a rapid expansion of existing urban areas has been registered worldwide, and the trend will become further intense as a response of population growth [1]. According to the United Nations, the current world population of 7.3 billion is expected to reach 8.5 billion by 2030, 9.7 billion in 2050 and 11.2 billion in 2100 [2]; two thirds of the population will live in urbanized areas by 2050 [3]. Many natural areas are converted to modern land uses such as buildings, roads and other impervious surfaces, increasing the complexity of urban landscapes. The physical interaction between urban morphology and the surrounding environment is strongly influenced by the geometry (i.e. orientations, height of the buildings and width of the street etc.) and the physical properties of the urban environment (i.e. streets, facades, roofs, etc.) [4]. Particularly, the features of these surfaces affect active and passive design strategies through exploiting the use of renewable energies sources (RES), the overall energy efficiency of buildings and the outdoor microclimatic conditions in urban areas. Therefore, the optimization of the use of urban surfaces is becoming crucial. This process should be performed in the early design phases considering the interaction with the built environment and the climate boundary conditions [5,6]. For example, the wind pattern can be potentially exploited for outdoor natural ventilation with direct (i.e. activation of urban airflows, cross ventilation in inner spaces and double skin façade (DSF) systems) and indirect (i.e. activation of wind vortex, decrement of outdoor surface temperature and humidity etc.) impacts at building and district scales [7]. Furthermore, the exposure and solar accessibility of the buildings' surfaces can be optimized to exploit the potential of the incoming solar radiation (i.e. direct, diffuse and reflected) [8,9]. Nevertheless, there is still a lack of knowledge on the best procedures to carry on this optimization, and, in particular, it is missing a holistic approach to conduct environmental and climate analyses and to transfer the outputs in design interventions.

1.1. *The advent and development of dynamic climate tools*

The assessment of performance for active and passive bioclimatic strategies can be more easily achieved during the early design phase of a design intervention. This can be done by combining numerical models capable of representing the geometrical complexity of actual urban configurations and the physical interactions among groups of buildings [10]. In this regard, the urban physical models, which started to be developed at the beginning of the 80's, were mostly focused only on one specific aspect of the urban climate and interaction at a time [11] due to the limited computational resources and the complexity of urban physics phenomena at district scale. Recently, the enhancement of available computational power has allowed the development of models able to reproduce and analyze almost the entire complexity of the urban physical phenomena (i.e. solar radiation, wind flows etc.) and the interactions inside the urban domain (i.e. urban canyon, group of buildings, districts etc.) by taking into account radiative behaviors, the complexity of district geometry, artificial and natural surfaces, and the physical properties of materials [11–14]. Given the advances in numerical models capabilities, one of the main concerns becomes to determine the physical interactions between the urban morphology and the surrounding environment, which strongly influence the microclimatic conditions in urban spaces [4]. This is a relevant factor to be considered in the optimization of urban surfaces (i.e. land, façades and roofs) to increase the overall energy efficiency of the district, produce energy from RES, and improve the outdoor thermal comfort in cities [15,16]. Aligned to this and compliant with the Energy Roadmap 2050 [17], a holistic approach would create win-win solutions by finding the best configurations to meet the European targets of sustainability for new and existing buildings and neighborhoods. In this scenario, where achieving energy-efficient and self-sustainable built environments is becoming more and more significant [18,19], it should become a common practice among urban planners and decision makers to explore the potential of RES to foster sustainable strategies at building and urban level throughout the whole design process from the early to the more detailed design phases.

This study aims to present such holistic approach applied in the early design phases on an urban case study in Bolzano (Italy). Sets of environmental analyses (i.e. solar energy and solar potential, wind flow, microclimate, etc.) have been conducted to study the mutual interactions among the different urban surfaces (i.e. buildings' facades, vegetation elements, soils and roads, etc.), to optimize the use of RES to assess passive and active bioclimatic strategies, and transfer the obtained results in design interventions and related technological solutions (i.e. high albedo materials, solar integrated systems (BIPV), green façade, DSF etc.) [5].

2. Background

2.1. *Geography and climate of Bolzano*

The city of Bolzano (UTM 46°29'53.8" N, 11°21'17.1" E) is situated in the North-East of Italy, in the center of the South-Eastern Alps in the administrative region of South Tyrol. Bolzano is located at a height of 265 m above the sea level in a basin surrounded by four mountain ranges. The significant height of the surrounding mountains impedes balancing currents and moisture. As a result, the city is characterized by a moist continental climate, Dfb according to the Köppen-Geiger classification [20], with strong seasonal fluctuations. Due to its location and climate characteristics, Bolzano is often affected by the presence of high temperature and extreme events such as heat waves during summer [21], and it is ranked among the hottest Italian cities with (dry-bulb) air temperatures (T_{air}) exceeding frequently 35 °C, with maximum peaks that reach 40 °C [22]. The analysis of the historical data series from 1950 to 2016 [22] shows an increase in the mean annual T_{air} of more than 3 °C (from 10.7 °C in 1977 to 13.9 °C in 2015) (Figure 1a) with the only exception in 1982, which resulted the hottest year in the series with the highest average annual T_{air} (13.9 °C). This maximum value was reached again in 2015. The analyzed trend is confirmed by a previous study conducted in the South Tyrol area [21], in which it was observed an increment of the annual average T_{air} by 1.5 °C in the last 30 years. The trend line (dotted line in Figure 1a) demonstrates that the temperature has constantly risen from 1950 to 2016. In the last 35 years (from 1981 to 2016) the increment is quite doubled, while looking at the trend line (dashed in Figure 1a) of the last 15 years (from 2001 to 2016) the increment is even higher.

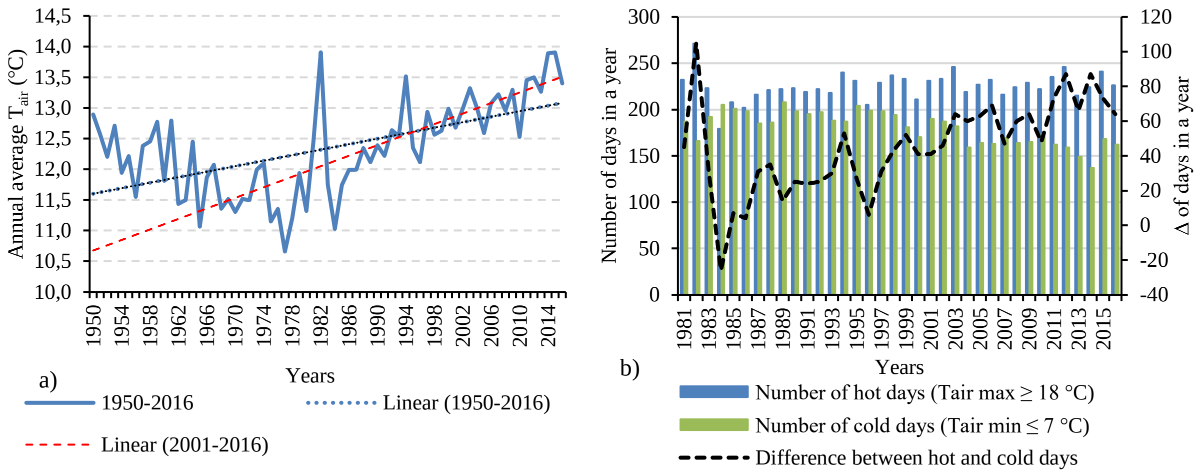

Figure 1 – (a) Annual average air temperature in Bolzano for the period 1950-2016. The dotted line represents the trend of the period 1950-2016; the dashed one is the trend line of the last 16 years, period 2001-2016. (b) Number of cold days ($T_{air\ min} \leq 7$ °C), hot days ($T_{air\ max} \geq 18$ °C) and the difference between the number of hot and cold days calculated considering the daily data of maximum and minimum T_{air} in the last 35 years (i.e. period 1981-2016).

The daily values of maximum and minimum T_{air} in the last 35 years (period from 1981 to 2016 [22]) (Figure 1b) were compared to the historical annual average of minimum (T_{air} = 7 °C) and maximum (T_{air} = 18 °C) T_{air}. The trend shows a relevant reduction of the cold days ($T_{air} \leq 7$ °C), while the hot days ($T_{air} \geq 18$ °C) are slightly incrementing. This means that the increment of the annual average temperature in Bolzano is mostly determined by an increase of the minimum T_{air}. This finding is also confirmed by the difference between the number of hot and cold days, which passes from 4 days in 1986 to 87 days in 2012 and 2014 (dashed line in Figure 1b) with two exceptions in 1982 and in 1984. The year 1982 was the hottest in the series, characterized by more than 270 hot days, with a positive difference of 105 days between hot and cold days, while the 1984 was the coldest year with more than 200 cold days and a negative difference between hot and cold days of 26 days in total. Furthermore, the increment registered for the minimum T_{air} is confirmed by the number of tropical nights (i.e. nights with $T_{air} > 20$ °C), which until the 1995 was less than five nights per summer, while in the last 20 years has increased significantly, reaching 20 tropical nights in 2010 [21].

The geographical location of Bolzano as well as the orography and its natural surroundings have also a relevant impact on solar potential and solar accessibility. The analysis of the direct, diffuse and global solar radiation elaborated from the *.epw* (*Energy Plus Weather*) data file of Bolzano [23] shows a quite typical annual solar distribution (Figure 2a). The monthly average value of the daily global solar radiation is always below 700 Wh/m^2, while the direct solar radiation overcomes the value of 400 Wh/m^2 only in June and July. This aspect is even clearer from the solar path: the intensity of global and direct solar radiation overcomes the thresholds of 1000 Wh/m^2 for global solar radiation and 700 Wh/m^2 for direct only few days during the summer season (Figure 3). However, the solar potential in Bolzano and its surrounding area results quite high as demonstrated by the numerous photovoltaic (PV) and solar thermal (ST) panels installation in public and private buildings [24].

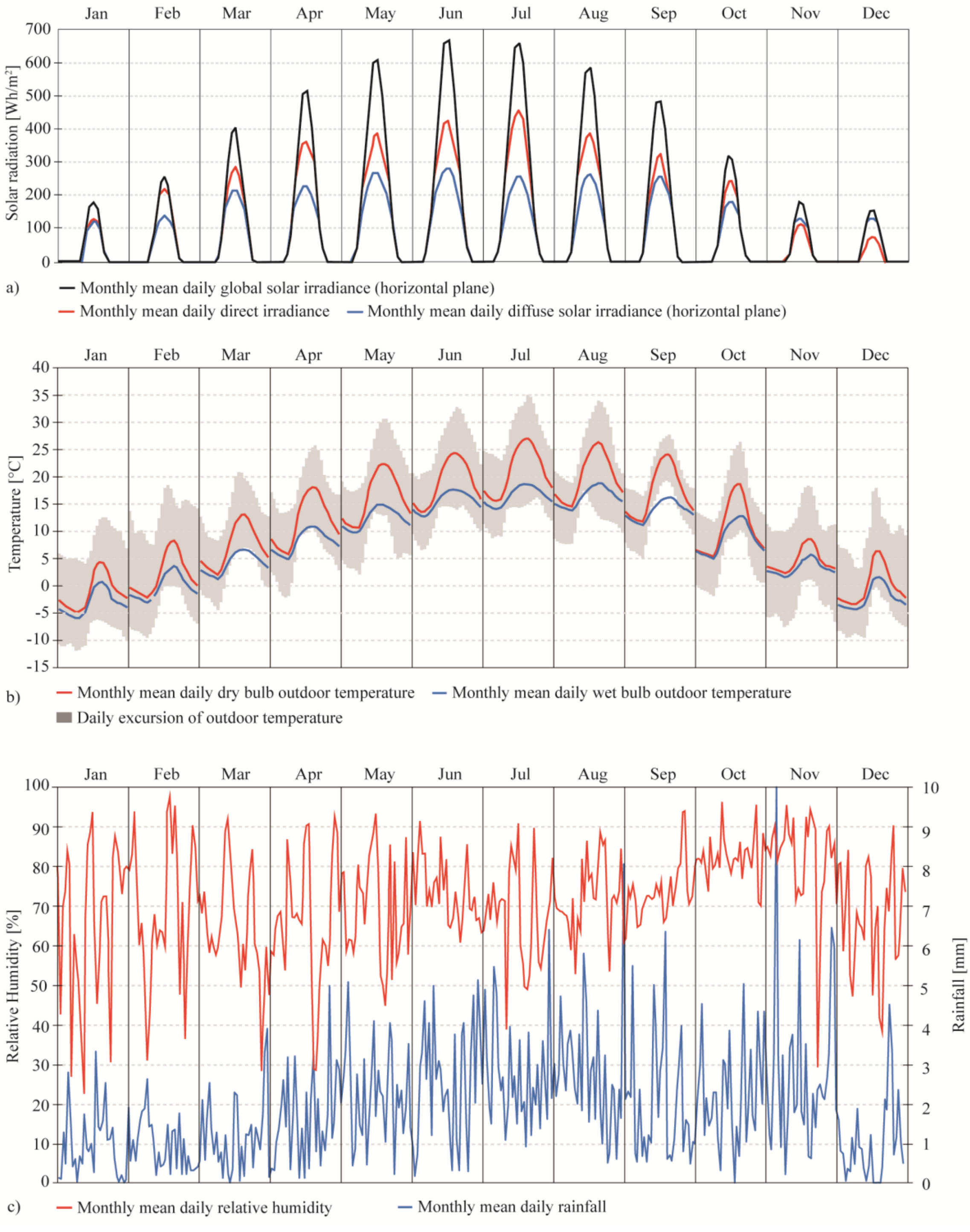

Figure 2 – Monthly mean daily trend of (a) global, direct and diffuse solar irradiance on a horizontal plane, (b) outdoor temperature and its daily excursion and (c) relative humidity and rainfall in Bolzano. Data elaborated from the .*epw* dataset of Bolzano with *Climate Consultant (version 6.0)*.

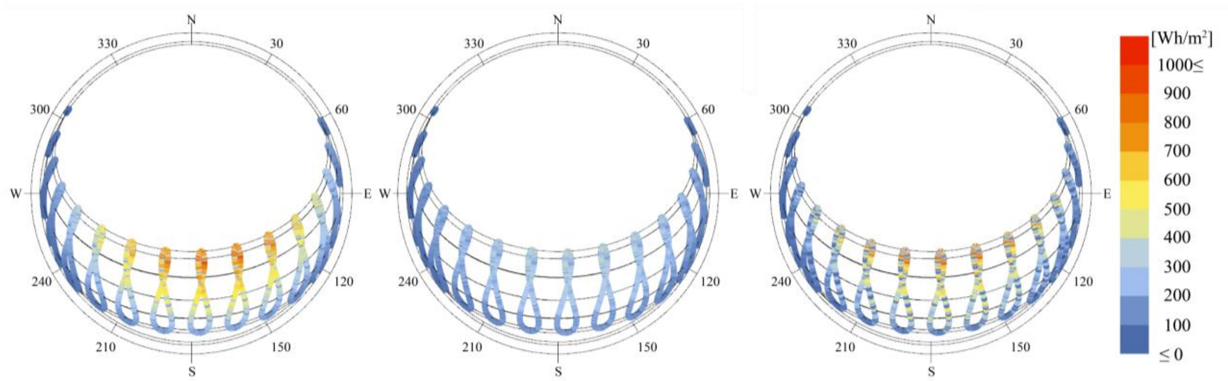

Figure 3 - (from the left) Solar path for global, diffuse and direct solar radiation in Bolzano (elaboration of the *.epw* with *Ladybug*).

Regarding the air temperature (Figure 2b), the monthly mean daily trend shows that July is the hottest month of the year, characterized by peaks of 35 °C and higher values for both dry bulb and wet bulb temperature, while the coldest months are December and January. May, June and November have high intensity of precipitation (Figure 2c). The wind speed (W_s) varies from the average value of 1 m/s in January to almost 6 m/s in May, with peaks in March, February and May, when the wind speed overcomes 30 m/s, 12 m/s and 10 m/s respectively (Figure 4). The annual analysis of the wind rose (Figure 5) underlines that the prevalent wind directions are North-East and South-East, while South-East and East are the prevalent wind directions during summer.

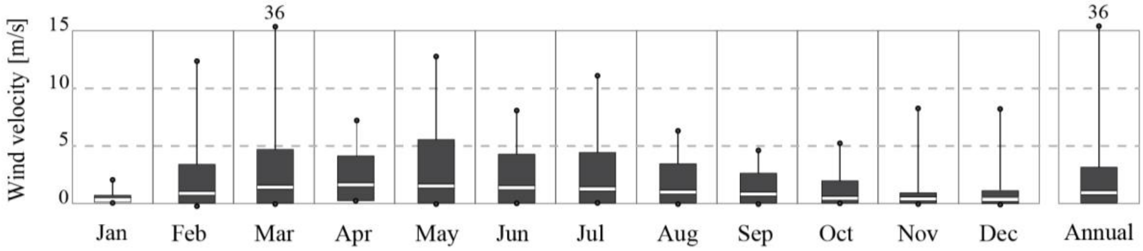

Figure 4 – Wind speed range in Bolzano (elaboration of the *.epw* with *Climate Consultant (version 6.0)*).

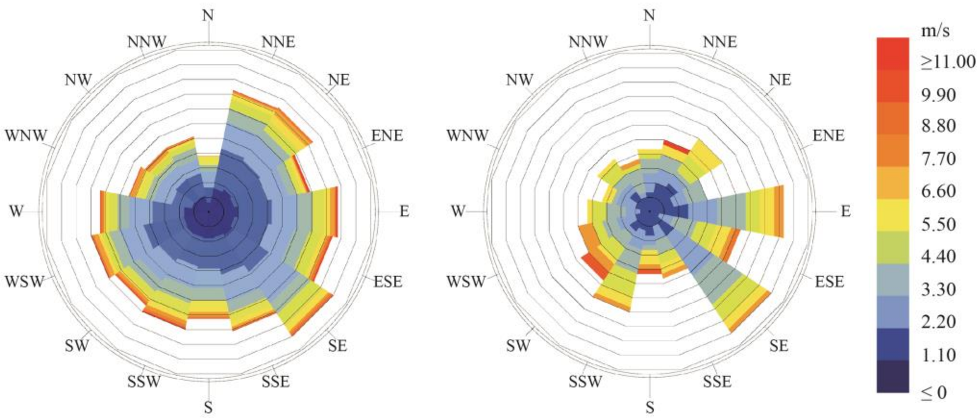

Figure 5 – Annual (left) and summer (right) wind rose in Bolzano (elaboration of the *.epw* with *Climate Consultant (version 6.0)*).

Given its location and its climate features, Bolzano represents an interesting case study. Furthermore, in the last years, the municipality of Bolzano has regulated energy standards towards the exploitation of RES [25] to foster energy efficiency of the buildings as well as to support the diffusion of active and passive bioclimatic strategies and to improve the outdoor human thermal comfort in existing neighborhoods.

2.2. *Case study area*

The urban area of Bolzano selected for this study is one of the case studies within the Smart Cities European project SINFONIA *(Smart Initiative of cities Fully cOmmitted to iNvest In Advanced large-scaled energy solutions*) that aims to deploy large-scale, integrated and scalable energy solutions in middle-sized European cities [26]. The district includes two residential building blocks (Bld_S1 and Bld_S2) of SINFONIA project and the nearby buildings (Bld_N1, Bld_N2 and Bld_N3). The area is delimited by five urban canyons: *Via Brescia*, *Garden*, and *Via Palermo* from West to East, and *Via Milano* and *Via Cagliari* from North to South (Figure 6).

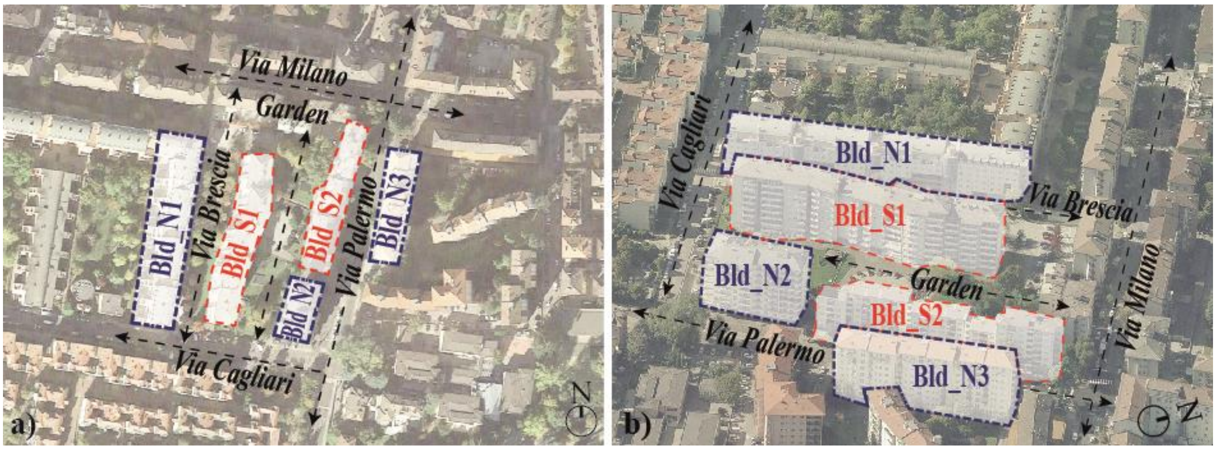

Figure 6 – (a) Top and (b) aerial view of the case study district (source: Google Earth).

Bld_S1, located in *Via Brescia*, is seven to eight floors above the ground and it is rotated by 8° clockwise from the North direction; while Bld_S2 faces *Via Palermo*, has from four to six floors and it is oriented 11.5° clockwise from the North direction. *Via Palermo* is one of the main access roads to the Eastern area of Bolzano, *Via Milano* and *Via Cagliari* are secondary roads, while *Via Brescia* is mainly used by the residents of Bld_S1 and Bld_N1 to access the underground parking areas. *Garden* is the central public area between Bld_S1 and Bld_S2 and is characterized by grass surfaces and by the presence of different species of plants and trees.

3. Methodology

The methodology implies sequential and logical steps (i) to develop an integrated workflow combining modeling and environmental analysis tools, and (ii) to address local climate aspects to optimize the use of urban surfaces' use (i.e. façades, roofs and ground) in consolidated urban environment. The workflow (Figure 7) starts with the analysis of the climate in Bolzano (Section 2.1) that allows to define the passive and active bioclimatic strategies on the site. The bioclimatic strategies are then tested in design scenarios representative of typical interventions conducted in European consolidated urban areas, in compliance with the objectives of the SINFONIA European project (Section 3.1).

The subsequent steps consists in three types of analyses conducted on the three-dimensional model of the case study district (Section **Error! Reference source not found.**) using dynamic climate tools and computational fluid dynamics (CFD) models:

1. Solar potential and solar accessibility analyses were evaluated on the two selected buildings for localizing the most radiate surfaces for solar systems' installation, and on the nearby buildings for identifying the most shaded façades (Section 3.5);

2. Microclimate analyses were run to define local climate conditions, and to estimate the impacts of the proposed design interventions (i.e. increment of albedo, addition of one story, and installation of a green façade) on the outdoor human thermal comfort (Section 3.6);
3. Qualitative airflow analyses were conducted to verify the use of natural ventilation in multifunctional façades (i.e. building integrated photovoltaic (BIPV), double-skin (DSF) etc.) and the activation of the "chimney effect" for the optimal roof inclination (Section 3.7).

In the last step, practice and policy implication for urban surface use in existing districts have been outlined.

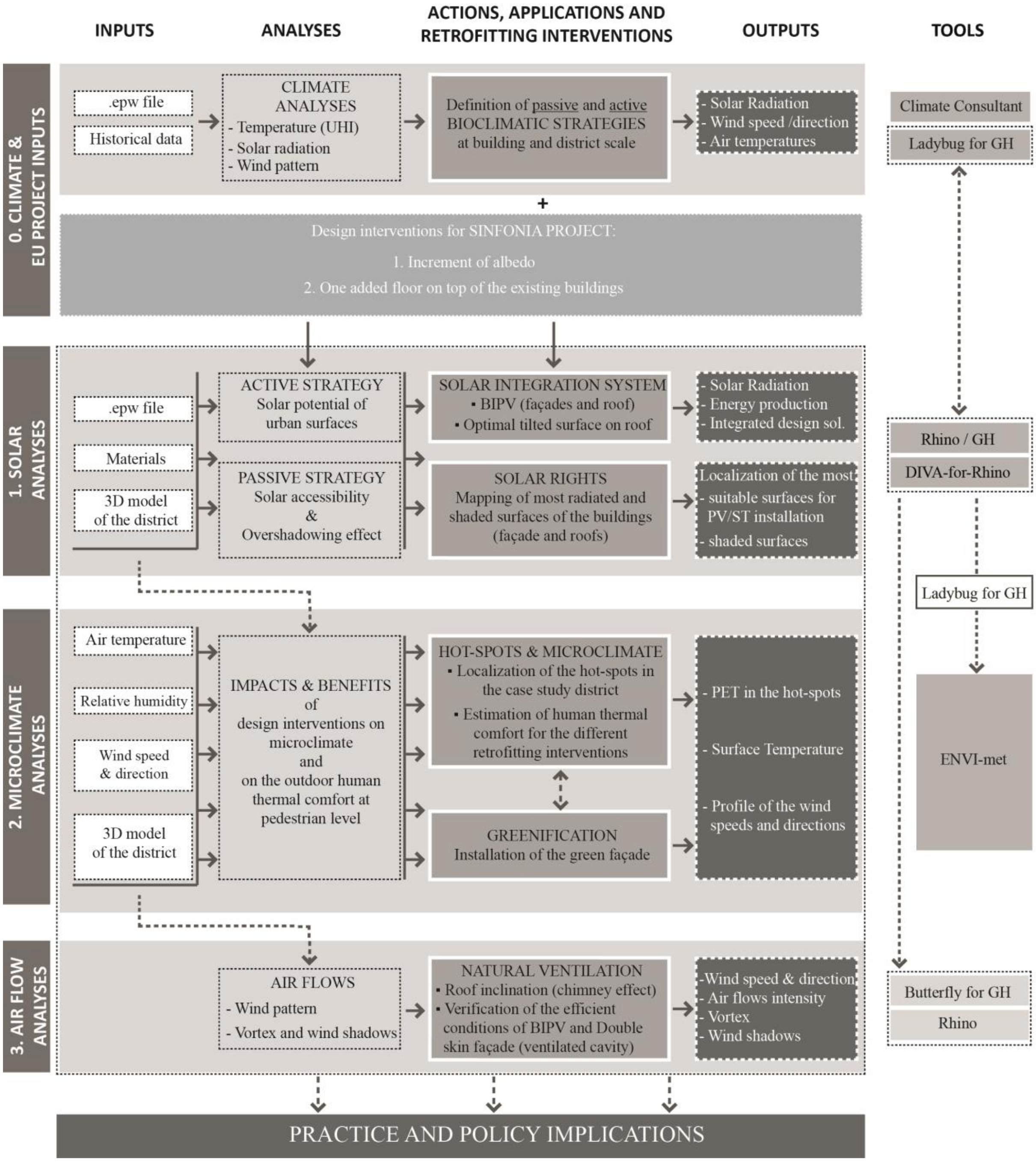

Figure 7 – Workflow of the presented methodology from the climate analysis and characterization of the city of Bolzano, to the analyses for solar, microclimate and ventilation strategies into the definition of practice and policy implications.

3.1. *Proposed design interventions on the case study*

In SINFONIA project, whole-building design and technological interventions which exploiting the use of RES (i.e. solar energy, wind, etc.) for active and passive bioclimatic strategies and the addition of volume (e.g.one story) have been undertaken [26]. This work aims to provide a holistic approach to guide designers throughout preliminary qualitative and quantitative environmental analyses to assess the impact of a set of design interventions. The design and technological interventions analyzed in the case study area are: (i) the replacement of the façades' finishing materials with different albedo or innovative technological solutions (i.e. multifunctional façade with BIPV, green façade, DSF, etc.), and (ii) the addition of one story volume on top of the existing buildings [27]. By conducting qualitative and quantitative environmental analyses, those interventions were considered in a wider complex urban environment.

3.2. *Climate analyses: tools and data*

A clear understanding of the local climate conditions of the site allows to determine active and passive bioclimatic strategies to optimize the use of urban surfaces. This work presents a local climate analysis (presented in Section 2.1) based on the elaboration of historical data series of Autonomous Province of Bolzano (from 1950 to 2016) [22], and on the use of climate tools such as *Climate Consultant* [28,29] and *Ladybug* [30]. *Climate Consultant* allows to read the hourly climate data of the whole typical reference year from the *.epw* file and to visualize the various weather attributes (i.e. radiation, wind, temperature, etc.) in graphic charts (i.e. dry- and wet-bulb temperatures, radiation and wind speed range bar chart, sun shading chart, psychometric charts and wind wheel). In order to complete the analysis of the local climate's characterization, the open-source weather analysis plug-in *Ladybug* [31] has been used. *Ladybug* allows to import the data from the *.epw* files into the environments of the Windows®-based NURBS modeler *Rhinoceros* [32] and the graphical algorithm editor *Grasshopper* [33]. *Ladybug* offers a variety of meaningful data visualizations in graphical charts and 3D interactive views, which can support designers in making more informed design assessment from the initial design stages. This approach expands the climate definition by simultaneously taking into account the implications between the built environment and the yearly weather data, as well as suggesting peculiar bioclimatic strategies for each specific location instead of relying on general rules [34]. It could be used from preliminary assessments of the site project, to the different phases of the design process in order to select both advanced bioclimatic strategies and environmentally-conscious design options at neighborhood, building and component scale.

3.3. *Procedure, reliability and uncertainties of the model*

One of the most critical aspects of modeling a real-world system is the guarantee of its physical fidelity, which means the model provides an accurate representation of the actual behavior of the system itself. However, since a model is a simplified representation of the real system, not all possible interacting phenomena that constitute the real-world can be analyzed at ones. As a result, a deviation exists between the outcome of the model and the real performance of the system. To keep such deviation under a tolerable level, quality assurance techniques are typically implemented. When the observations of the real behavior of a system are available, it is possible either to calibrate a model to reduce its overall uncertainty or to evaluate the quality of a model with validation.

In our case, no physical measurements were available neither to calibrate our models nor to validate them; therefore, a strict procedure was adopted to control all the steps of the model development in order to reduce all possible epistemic uncertainties. Furthermore, the typical meteorological year weather data were used to fix the aleatory uncertainty related to the description of the climate boundary conditions in all the developed models. Specifically, the adopted modeling procedure, already used for another modeling and simulation analysis [35], consists in seven steps:

1. All of the modeling specifications were collected and assembled in a design package.
2. The design package was delivered to two independent modelers, who worked in absolute autonomy and avoided any reciprocal contact or interference while developing the numerical models.
3. The main performances were identified for each type of model and used as benchmarks.
4. After the simulation runs, a graphical comparison of the benchmarks was carried out using scatterplots.
5. The bias between each couple of models was quantified using the mean bias error, and the overall uncertainty was evaluated using the coefficient of variation of root mean square error.
6. When a discrepancy was found between two models, an independent comparison of the input variables of the models was carried out to identify the sources of discrepancy that caused the deviation in the benchmark.
7. Finally, the errors were fixed, and the reference models were finalized and used for the subsequent analyses.

Of course, this modeling procedure cannot guarantee that the simulation outcomes reflect the actual performance of the urban district (physical fidelity), but it can help to minimize epistemic uncertainty, in particular specification and modeling uncertainties.

3.4. *Modelling of the case-study area*

The three-dimensional model of the case study district was created using *Rhinoceros* and *Grasshopper*. Buildings and ground surfaces were modelled directly in *Rhinoceros* by reproducing the geometric proportions between the height of the building (H) and width of the street (W), which define the aspect ratio (H/W) of each urban canyon, while a *Grasshopper* script was used to create the trees. The dimensions of the tree's crown on the three axes (x, y, z) was modelled as a hollowed sphere, whose structure is composed by a texture with alternating void and surfaces (Figure 8b). The percentage of voids in the surface was based on the Leaf Area Index (LAI) of the different species of trees existing in the district.

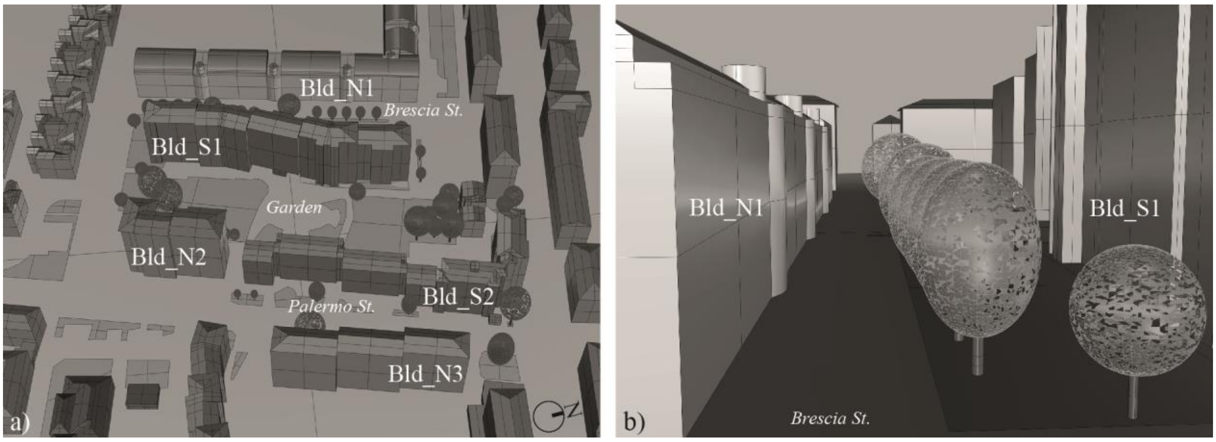

Figure 8 – (a) View of the three-dimensional model of the entire case study district. (b) Visualization the tree-lined street in *Via Brescia* modelled with *Grasshopper* script and exported in *Rhinoceros* environment.

3.5. *Solar analyses: objectives, inputs and tools*

The solar analyses were conducted at the district scale in order to:

i. Generate solar radiation map to identify the most irradiated buildings' surfaces and to calculate their solar potential;

ii. Quantify the impacts of the proposed design interventions on the surrounding buildings in terms of mutual solar reflections and overshadowing effect.

The sets of solar simulations were run by coupling *Rhinoceros* and *Grasshoppe*r with the solar dynamic simulation tool *DIVA-for-Rhino,* which is a validated *Radiance-Daysim/* based software able to simulate the annual amount of daylight in and around buildings [36]. In order to demonstrate the reliability of the software, a previous study, where experimental data on site have been compared with simulated outcomes, was analyzed. In Table 1 are reported the Relative error (Rel_{err}), Mean Bias Errors (MBE) and Root Mean Square Errors (RMSE) between the measured data and the simulation conducted for annual and monthly irradiation on the South façade of buildings in different urban scenarios. With the exception for the 2.0 m-height sensor located in a complex urban environment, for which RMSE results up to 125 %, the results demonstrate that *Daysim* is able to track the yearly and monthly profile of irradiation for an unobstructed sensor with a reasonable accuracy: Rel_{err} < 5%; MBE < 5% and Cv(RMSE) < 30%.

Table 1 – Results of experimental validation carried out in previous studies using Daysim as calculator engine. All the values of Abs_{err}: absolute error, Rel_{err}: relative error, MBE: mean bias errors; RMSE: root mean-square error, are related to a South-oriented façade.

City	**Area**	**Variable [unit]**		**Abs_{err} [kWh/m^2]**	**Rel_{err} [%]**	**MBE [%]**	**RMSE [%]**	**Ref.**
Freiburg, Germany	Unobstructed building	Annual irradiation [kWh/m^2]		-6	-0.8			[37]
		Monthly irradiation [kWh/m^2]				-0.7	21	
New York, US	Dense urban context	Annual irradiation [kWh/m^2]	2.0 m	-3				
			100 m	-10				
			220 m	-7				
		Monthly irradiation [kWh/m^2]	2.0 m		-0.5	-4.0	127	
			100 m		-4.8	-1.0	37	
			220 m		-0.7	0.0	17	

The *Daysim* calculation engine of *DIVA-for-Rhino* uses typical *.epw* weather data file for a specific site location to obtain climate-based daylighting metrics [38]. For the present work, the *.epw* weather data file of Bolzano was employed. In order to increase the computational accuracy, the annual global and direct solar radiations incident at the buildings' envelopes were calculated using the grid-based radiation method. The *Radiance* parameters' settings (Table 2) to perform the simulations were taken from previous similar studies [8,39].

Table 2 **–** Set of 'rtrace' parameters used for all *Radiance*-based simulations.

Ambient bounces	**Ambient division**	**Ambient super samples**	**Ambient resolution**	**Ambient accuracy**	**Specular threshold**	**Direct sampling**	**Direct relays**
1–3	1000	20	300	0.1	0.15	0.20	2

In order to compute the interaction between solar radiation and urban morphology, custom *Radiance* materials were defined for each surface (i.e. ground, façade, roof and vegetation) of the district (Table 3). The materials' properties were set considering the parameters of color (RGB values), specularity (fraction of incident light that is reflected; varying from 0.0 for a perfectly diffusive surface to 1.0 for a perfect mirror), and roughness (surface irregularities quantified by the deviation from its ideal direction of the normal vector of a real surface; the value varies from 0.0, which corresponds to a perfectly smooth surface, to 1.0 that corresponds to a perfectly irregular surface [40]). In this study, specularity and roughness were set to 0.0 for all the materials. The reflectance value 0.95 (OutsideFaçade_100%R), has been chosen as maximum albedo for building outside façades, considering that modern reflective finishing materials can reach a maximum albedo of 0.96 [41].

Table 3 **–** List of materials properties used in *Radiance*.

	Radiance material	**Materials / colors**	**Radiance material**	**Number of arguments**	**RGB reflectance/albedo**	**Effective reflectance values**
Veg	Vegetation_10%R	Wood	Void plastic	0 0 5	0.10	0.10
	Vegetation_40%R	Foliage	Void plastic	0 0 5	0.40	0.39-0.51
Ground	OutsideGround_20%R	Asphalt	Void plastic	0 0 5	0.20	0.19
		Concrete				0.23
		Loamy soil				0.05–0.25
		Grass				0.16–0.26
Façades	OutsideFaçade_30%R	Paint brown	Void plastic	0 0 5	0.30	0.22-0.36
	OutsideFaçade_40%R	Paint beige red	Void plastic	0 0 5	0.40	0.42
	OutsideFaçade_50%R	Paint yellow	Void plastic	0 0 5	0.50	0.43
		Paint cream white				0.42-0.54
	OutsideFaçade_70%R	White ceramic	Void plastic	0 0 5	0.70	0.72-0.77
	OutsideFaçade_100%R	Reflective paint white	Void plastic	0 0 5	0.95	0.80–0.95
Roof	GenericCeiling_10%R	Dark grey concrete tiles	Void plastic	0 0 5	0.10	0.10-0.15
	GenericCeiling_30%R	Grey concrete tiles	Void plastic	0 0 5	0.30	0.31–0.33
	GenericCeiling_70%R	Red ceramic tiles	Void plastic	0 0 5	0.70	0.68

3.5.1. *Scenarios of solar analyses*

The solar analyses were conducted in four scenarios (Table 4), accounting for different sets of design interventions applied on buildings and urban canyons (Table 5).

Table 4 **–** Design scenarios adopted for the solar analyses.

Scenario	**ID**	**Analyzed buildings (Bld_S1 and Bld_S2)**		**Nearby buildings**
		Height	**Façade material**	
Baseline Scenario – Current albedo	BS_CA	Unvaried	OutsideFaçade_50%R	Unvaried
Baseline Scenario – High albedo	BS_HA		OutsideFaçade_100%R	
Added Story Scenario – Current albedo	AS_CA	Increment of one story volume	OutsideFaçade_50%R	
Added Story Scenario – High albedo	AS_HA		OutsideFaçade_100%R	

Table 5 **–** Features of the urban canyons in the baseline (BS) and added story (AS) scenarios.

Urban Canyon	**Buildings and streets features**				**H/W**	
	Height of the buildings [m]		**Width of the street [m]**			
	BS	**AS**	**BS**	**AS**	**BS**	**AS**
Via Brescia	24.5	27.5	29	29	0.84	0.95
Garden	24.5	27.5	44	44	0.56	0.63
Via Palermo	14.7	17.7	24.5	24.5	0.60	0.72

In the baseline scenario (BS_CA), the albedo of the façades and the height of Bld_S1 and Bld_S2 were maintained unvaried from the actual situation in order to quantify the incident direct (Irr_{dr}) and global (Irr_{gl})

radiation levels at the building envelope. The obtained results were used as reference values for comparison with the other scenarios. In the baseline scenario with high albedo (BS_HA) and in the added story scenario with high albedo (AS_HA), the finishing materials of the façades of buildings Bld_S1 and Bld_S2, were modified in the numerical model to vary their reflectance from 0.5 (façade albedo in the current situation) to 0.95 (completely reflective). The variation of Irr_{gl} at the building envelope was evaluated for both Bld_S1 and Bld_S2 and nearby buildings Bld_N1, Bld_N2 and Bld_N3. The twofold impact given by the increment of one story volume of Bld_S1 and Bld_S2 was studied in the added story scenario with current albedo (AS_CA), in order to estimate the (i) overshadowing effect on the nearby buildings, Bld_N1 and Bld_N2, and the (ii) availability of buildings' surfaces with high solar potential for installing solar active systems. Successively, in the AS_HA scenario, the analyses were focused on the influence of mutual solar reflections given by the increment of the façades albedo. In all scenarios, the reflectance value of the ground was set equal to 20% (i.e. average value for ground materials, whose reflectance is around 19% for asphalt and varies from 16% to 26% for grass), while the materials' properties of the nearby buildings were maintained unvaried. The simulations were run to identify: (i) the most irradiated façades of buildings Bld_S1 and Bld_S2 suitable for installing solar systems, and (ii) the most shaded façades of the surrounding building Bld_N1, Bld_N2 and Bld_N3 due to the added story in both AS_CA and AS_HA scenarios. These analyses allowed to estimate, in the scenario with the added volume of one story, if the solar potential and solar accessibility along the façade are effectively suitable for the installation of solar systems (PV and ST) in different periods of the year (i.e. cold season autumn and winter and hot season spring and summer).

3.6. *Microclimate analyses: objectives, scenarios, inputs and tools*

The microclimate analyses were focused on the following objectives:

i. Identify the hot spots areas with high level of human thermal stress in the urban canyons in the baseline scenario BS_CA;
ii. Assess the thermal impacts of different finishing materials albedo in BS_HA and AS_HA scenarios, and of the increment of the added story volume in the scenario AS_CA;
iii. Estimate the benefits of green façade as mitigation intervention in proximity of the hot spots.

In order to accomplish these purposes, the numerical model *ENVI-met*, version 4.0, has been used. *ENVI-met* is a 3D prognostic microclimate model designed to simulate the surface–plant–air interactions in urban complex environments with spatial resolution of 0.5–10 m and temporal resolution of 10 s [11]. The model physics is based on non-hydrostatic Navier-Stokes equations (for wind flow computation), thermodynamics laws (for calculation of temperature fields), and atmospheric physics (for prognosis of atmospheric turbulence) [42,43]. *ENVI-met* allows (i) to set the grid size resolution small enough to reproduce buildings; (ii) to compute the energy balance for all surfaces in the model; (iii) to simulate the physical and physiological properties of vegetation; (iv) to calculate the atmospheric processes (wind flow, turbulence, exchange processes of heat and vapor at urban surfaces, exchanges of energy and mass between vegetation and its surroundings) with a prognostic and transient method.

A literature review on *ENVI-met* (version 4) validation studies has been conducted to evaluate the degree of approximation of the simulated results with respect to actual field measurements. Table 6 reports the results of the experimental validations. The analysis of the statistical errors outlines a satisfying correspondence between the numerical simulations and experimental observations for T_{air}, R_H, and T_s. Higher values of RMSE are noticeable for T_{mrt} and Irr_{gl}. However, in general, *ENVI-met* can guarantee appropriate results for a preliminary assessment of the microclimatic implications of design interventions as it is the scope of the present study.

Table 6 – Results of experimental validation carried out in previous studies conducted with *ENVI-met*. R^2: coefficient of determination - RMSE: root mean-square error - RMSD: root mean-square deviation - d: index of agreement.

City	Area	Variable [unit]	R^2	RMSE	RMSD	d	Ref.
Hannover, Germany	Center of semi-closed courtyard	T_{air} [°C]	-	0.73	-	-	[44]
		RH [%]	-	3.34	-	-	
		W_s [m/s]	-	0.01	-	-	
		T_{mrt} [°C]	-	8.44	-	-	
Thessaloniki, Greece	Urban district	T_{air} [°C]	-	-	1.85	0.90	[45]
Rome, Italy	Cloister of Saint Peter in Chains	T_{air} [°C]	0.88	1.89	-	0.91	[46]
		T_{mrt} [°C]	0.96	2.79	-	0.87	
Freiburg, Germany	Residential district	T_{air} [°C]	0.85	0.66	-	0.95	[47]
		T_{mrt} [°C]	0.86	5.49	-	0.95	
São Paolo, Brazil	High density district	T_{air} [°C]	-	1.75[a]	-	0.89[a]	[48]
Bilbao, Spain	Four urban areas with different urban climate	T_{air} [°C]	0.96[a]	-	-	-	[49]
		T_{mrt} [°C]	0.71[a]	-	-	-	
Guangzhou, China	Open area of future construction site	T_s [°C]	0.97	1.98	-	0.99	[43]
		T_{air} [°C]	0.94	1.01	-	0.97	
		Irr_{gl} [W/m^2]	0.91	28.3	-	0.97	

[a] Mean value

The 3D model of the case study district (Figure 9) modelled in *Rhinoceros* was exported in *ENVI-met* by using the *ENVI-met* components of the *Ladybug* plug-in for *Grasshopper*. The surfaces of the buildings' model were simplified to reduce the computational time needed to process all information.

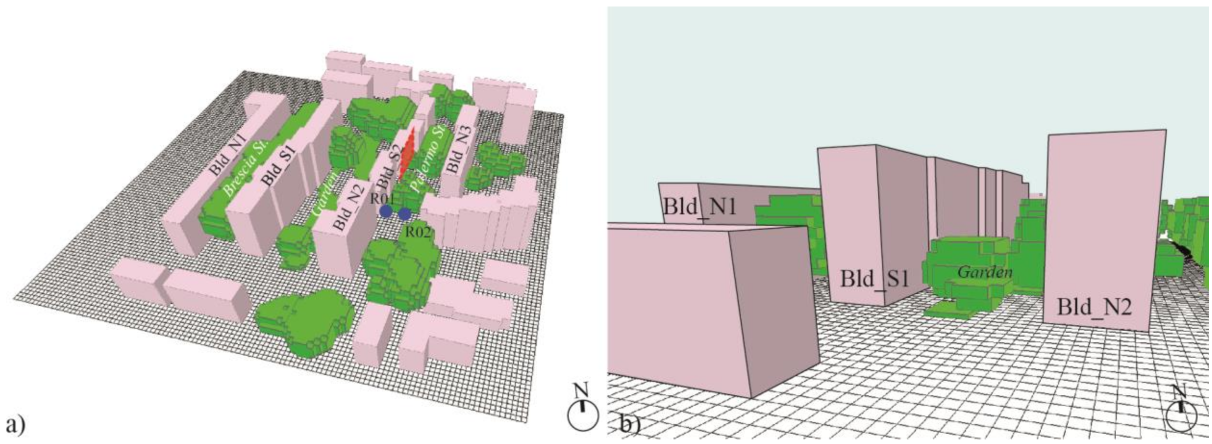

Figure 9 – (a) Three-dimensional model of the entire district. The position of the green façade is highlighted in red. (b) Visualization of Garden modelled in ENVI-met environment.

On this regard, all the buildings share flat roofs and same finishing materials properties. Aerial images and photos taken on-site were used to check the property of buildings (i.e. height, finishing materials etc.), plants (i.e. type, height, volume etc.) and ground (i.e. grass, asphalt, etc.).

Thermo-physical properties were selected according to UNI 11300 [50] based on the year of buildings' construction (1978 for Bld_S1 and 1960 for Bld_S2), while typical optical properties were chosen based on construction and thermal-imaging manuals. The properties of the ground were taken from default *ENVI-met* database. Table 7 summarizes the materials features of buildings and artificial surfaces used in *ENVI-met* model.

Table 7 – Features of artificial surfaces set in *ENVI- met* model.

	Buildings		Ground		
Material Type	Concrete/external plaster	Concrete	Asphalt	Concrete	Dirty Concrete
Allocation	Walls	Roofs	Streets	Pavement	Pavement
Thickness [m]	0.40	0.30	0.10	0.30	0.30
Absorption Irr_{SW} Absorbed Fraction	0.40	0.70	0.60	0.50	0.60
Reflection Irr_{SW} Reflected Fraction	0.60	0.30	0.40	0.50	0.40
Emissivity Irr_{LW} Emitted Fraction	0.96	0.90	0.90	0.90	0.90
Specific heat [J/kg K]	900	840	650	840	840
Thermal conductivity [W/m K]	0.40	0.86	0.50	0.20	0.20
Density [kg/m^2]	750	930	1500	620	620

In order to align the model to the district's orientation, it was rotated by 11.5° clockwise from the North direction. The area was digitized with a resolution of 2 m in all directions, resulting in model area size of 110 x 115 x 30 grids and a domain extent of the modelled area equal to 220 x 230 x 60 m. In order to reduce the influence of climatic boundary conditions at the borders of the model domain, a total number of eight nesting grids with a coarser resolution was set.

Table 8 – Inputs data for the configuration of the *ENVI- met* model and outputs of the analysis.

Start date and duration of simulation	Start date	July 20th at 04:00
	Total simulation time [h]	44
Initial meteorological conditions	W_s at 10 m height [m/s]	2.53
	Wind direction	South-East
	Initial temperature of atmosphere [°C]	30
	Specific humidity at model top (2500 m, [g/kg])	2.92
Simple forcing setup Hourly data from meteorological station.	T_{air} [°C]	min($T_{air\ @\ 6:00}$) = 24.3; max($T_{air\ @\ 15:00}$) = 38.3
	RH [%]	min($RH_{@\ 16:00}$) = 24; max($RH_{@\ 16:00}$) = 69
Solar radiation and clouds	Adjustment factor for solar radiation	1.00
	Cover of medium clouds [octas]	2.00
Outputs of the analysis	Total wind speed	W_s [m/s]
	Direction of the air flow	Wind direction [°]
	Relative Humidity Air	RH [%]
	Air temperature	T_{air} [°C]
	Mean radiant temperature	T_{mrt} [°C]
	Surface temperature	T_s [°C]

The microclimate conditions were analyzed for the hottest day of 2015, July 21st, which was chosen as representative of a typical hot summer day in Bolzano. Climate data of air temperature (T_{air}), relative humidity (RH), average wind speed (W_s), and prevalent wind direction were collected from a weather station located on the city hospital roof at a distance of 1.7 km North/West from the district case study area. Those input data were used in *ENVI-met* to "force" the model by providing the inflow boundaries (Table 8). The start of the simulations was set at 4:00 am of the previous day (i.e. 20th of July) since the numerical model needs at least 20 hours of initialization time [51,52] to overcome the initial transient conditions and to not affect the reliability of the results of the analyzed day (i.e. 21st of July). Therefore, the resulting simulation time was 44 hours. The microclimate analysis and screening of hot spot areas was carried out at pedestrian level, at 1 m above the ground.

3.6.1. *Scenarios of microclimate analyses*

The scenarios defined in Table 4 were also tested in the microclimate analyses, focusing on the localization of the hot spots in the case study district and the impact of the proposed interventions on human thermal comfort, while a new scenario related to the installation of a green façade (scenario named as Gr_Fac) was studied. In that regard, two receptors (Figure 9a) were set in *ENVI-met* environment: R01 positioned in the proximity of the green façade, and R02 located in the proximity of a hot spot in *Via Palermo*. The vertical greening system was modelled with climber species represented well-grown but not completely covering the façade. However, given that *ENVI-met* presents some limitations in modeling vertical greening systems [53], the façade was modelled as a row plant of 0.5 m width and 16 m height, which correspond to the dimension of the analyzed façade of the Bld_S2. Additionally, the leaf area density (LAD) was set to 1.85 m^2/m^3, as in previous studies [54,55]. This LAD value is representative of *Parthenocissus tricuspidata*, a climber specie common in Southern Europe, which attaches itself to vertical surfaces with or without technical climbing support. These plants are usually rooted on a substrate of loamy soil that was also set in *ENVI-met* as ground type.

3.6.2. *Index for thermal human comfort analysis*

The human thermal comfort at pedestrian level in the urban canyons of *Via Brescia*, *Via Palermo* and in the *Garden* was evaluated by means of the meteorological parameters that have a thermophysiological effect on a human being, that are T_{air}, RH, W_s, T_{mrt}, T_s, and the pedestrians' metabolic activity and thermal resistance of clothing. In this study, outdoor thermal conditions are expressed for a male of 35 years, who is 1.75 m high and weighs 75 kg, and are assessed with the Physiological Equivalent Temperature (PET). The PET is a thermal index developed by Höppe to assess thermal comfort in outdoor environments [56–58]. This index is based on the Munich Energy-balance Model for Individuals (MEMI) [59] and is defined as the "air temperature at which, in a typical indoor setting (i.e. without wind or solar radiation), the heat budget of the human body is balanced with the same core and skin temperature as under the complex outdoor conditions to be assessed" [56]. In the calculations, the thermal resistance of clothing is set at 0.90 clo and the metabolic heat production (H) is set at 80 W m^2. These two individual variables are assumed constant to isolate the evaluation of the atmospheric components from the influence of personal choices. PET is one of the most diffused index in outdoor thermal comfort studies due to its measuring unit (i.e. °C), which makes the results readily comprehensible to everyone [60]. The *ENVI-met*´s post-processing tool *BioMet* was used to calculate PET for the evaluation of thermal comfort in the outdoor environment, in compliance with the German standard VDI 3787-Part 2:2008 [61].

3.7. *Airflow analyses: objectives, inputs and tools*

In this study, the CFD simulations aimed to qualitatively:

i. Verify the efficiency of optimization process in the operating conditions of double-skin façade (DSF) coupled with Building integrated Photovoltaic (BIPV) systems installed on the East façade of the buildings Bld_S1 and Bld_S2;
ii. Verify the activation of the "chimney effect" for the optimal roof inclination on the Bld_S1.

The study of the ventilation pattern (i.e. direction and speed) of outdoor airflows on the building's façades implied 3D steady RANS (Reynolds Averaged Navier-Strokes) Computational Fluid Dynamics (CFD) simulations, which were conducted with Re-Normalisation Group (RNG) κ-ε turbulence model ($C\mu = 0.0845$)

using *OpenFOAM*, an open source validated engine for CFD analyses [62]. In this regard, Table 9 collects some previous studies that have used the same CFD and turbulence model and have compared the simulated outcomes with real experimental data. The results underline a pretty good convergence between simulation and wind tunnel experimental data with the distributed errors varying from 25% and 55%. However, the model's accuracy works properly for the purpose of this work, in which simulations have been conducted to preliminarily and qualitatively assess the goodness of possible design interventions.

Table 9 – Results of experimental validation carried out in previous studies conducted with *OpenFOAM*.

Focus of the study	**Validation data**	**CFD and turbulence model**	**Variables analyses**	**Results**	**Ref.**
Natural ventilation for agricultural buildings	Wind tunnel experimental data	RANS with standard κ-ε model	Mean relative error bounded (%) with respect to the convergence of simulations.	Convergent. Errors distributed from 25% to 45%.	[63]
		RANS with RNG κ-ε model		Convergent. Errors distributed from 25% to 40%.	
		RANS with realizable κ-ε model		Not converged. Errors distributed in high values (35-70%)	
		RANS with low *Re* κ-ε model		Convergent. Errors distributed from 25% to 55%.	
Airflow around a single high-rise building	Wind tunnel experimental data	RANS with standard κ-ε model	Reattachment lengths	$x_F/b = 2.68$ overestimated (experimental result: $x_F/b = 1.42$) $x_R/b = 0.52$ in good agreement (experimental result: $x_R/b = 0.50$)	[64]
External flows in urban environment			Wind speed ratios	Results fall outside the one standard deviation band in 24 out of total 60 tests.	
Airflow distribution of single-sided ventilation in building	Wind tunnel experimental data	RANS with standard κ-ε model	Normalized streamwise mean velocity	Good agreement between experimental values and simulation results.	[65]
			Normalized vertical mean velocity	The trend of RANS model is less accurate compared to the experimental values.	

In order to account for buoyancy, the Boussinesq approximation was adopted. The vertical profiles of the mean horizontal wind speed were imposed at the inlet of the computational domain equal to 2.53 m/s from the prevalent wind direction South-East, at the reference height of 10 m, and for a roughness length of 6 [66]. The dimensions of the computational domain were set to 3 H upstream and 15 H downstream, where H is the height of the tallest building in the district. Along the vertical direction, the domain was set 3 H height, while in the lateral direction it was extended for a further width of 2 H on each side. In order to run the CFD simulations in *Rhinoceros* environment, the plug-in *Butterfly* was used. *Butterfly*, within the *Ladybug* family software, is a light python Application Programming Interface (API) for *Grasshopper* that creates and runs cases in *Rhinoceros* environment by using *OpenFOAM* as external validated simulation engine [67]. The computational domain was discretized with a mesh of around 2 million cells, which was generated in two steps. First, the utility *BlockMesh* was used to create a simple block mesh based on fully-structured hexahedral cells, which defined the extent of the computational domain and a base level mesh density. Successively, the mesh was refined by using the utility *SnappyHexMesh*, which generated a high-quality tree-dimensional hex-dominant mesh, adding layers for wall resolution. Using this utility, the refined cells near the buildings were split up to six times for increasing the mesh density in proximity to the obstacles for reducing numerical instability, errors and uncertainty. To balance the computational time with the calculation accuracy, the *multi-grading* option was employed to progressively increase the mesh cell dimensions farther from the building geometry in the region outside the district. The expansion ratio of adjacent grids cells was set to 1.2 for all the directions, as suggested by Franke [68]. Finally, the sections' planes AA' and BB' (Figure 10) were set in order to plot the results.

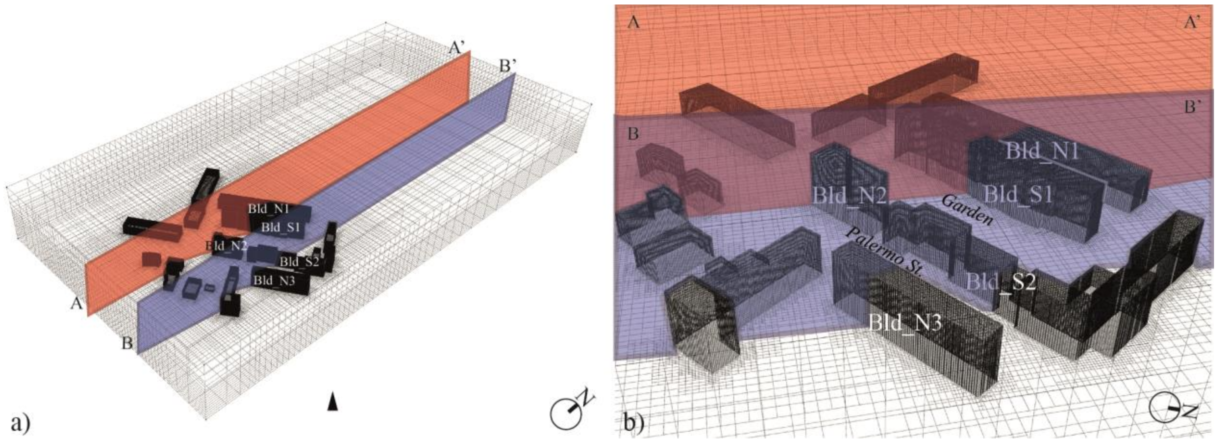

Figure 10 – (a) View of the three-dimensional domain of the wind tunnel; (b) Visualization of the refined mesh grid near the buildings.

Inside the domain a simplified 3D model of the selected district was created as input for the geometrical representation of buildings' shapes and dimensions, including the buildings Bld_S1 and Bld_S2 and the nearby buildings (Bld_N1, Bld_N2 and Bld_N3) (Figure 10).

3.7.1. *Scenarios of urban airflow analyses*

Three different scenarios were analyzed: (i) the baseline scenario (BS_CA), (ii) the added-story scenario (AS_CA) as defined in Table 4, and (iii) a new scenario that combines the added-story volume with the application of a DSF coupled with BIPV (AS_DSF_BIPV). The AS_DSF_BIPV scenario was considered as a feasibility study to verify the efficiency of DSF installation coupled with BIPV on the East façades of both buildings Bld_S1 and Bld_S2. The façade was designed at a distance of 0.7 m from the existing building envelope with the upper part tilted by 38° from the horizontal plane in order to estimate (i) the wind fluxes in the air cavity and (ii) the efficiency of the building integrated solar systems. According to the calculation in *PVGIS* [69], the geometrical configurations to optimize the incident solar radiation on a surface located in Bolzano are a tilt angle of 38° from the horizontal plane and an azimuth of 7.5° towards the West direction.

4. Results and discussion

The relevant results related to the analyzed scenarios are discussed along with the significance of addressing both the proposed design interventions on buildings Bld_S1 and Bld_S2 and the impacts on the nearby buildings Bld_N1, Bld_N2 and Bld_N3.

4.1. *Solar analyses*

The outcomes of the solar analyses were focused on two assessments: (i) the solar potential of Bld_S1 and Bld_S2, and (ii) the impact of the design interventions on the nearby building Bld_N1.

4.1.1. *Solar potential analyses on the SINFONIA buildings*

The solar analyses conducted on the two buildings Bld_S1 and Bld_S2 have focused on the estimation of their solar potential. In Bld_S1 the most irradiated façades are those facing East (E in Figure 11a) and South (S in Figure 11a). Due to its orientation, the South façade is not influenced by the variation of height and albedo. With values of direct radiation around 320 kW h/(m^2 a), from the fourth floor up the façades resulted suitable for installing solar systems in all the simulated scenarios.

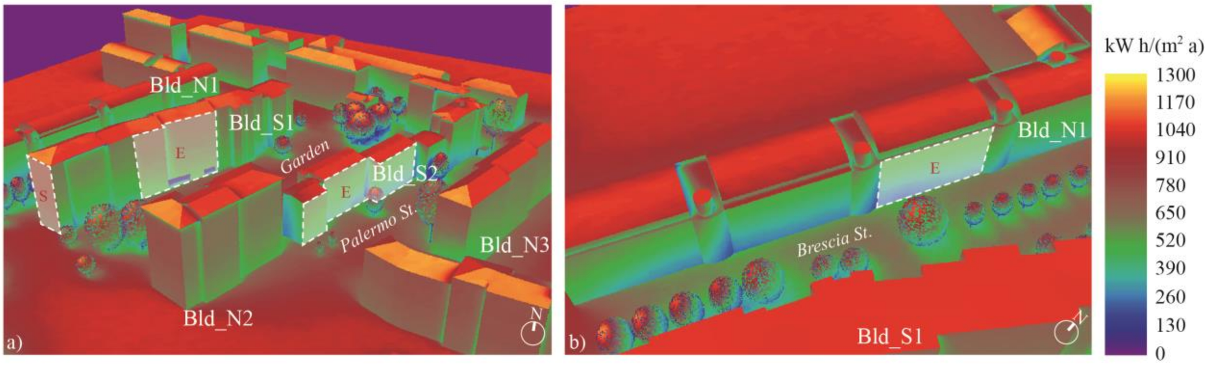

Figure 11 – Radiation maps with identification of the analyzed façades. (a) East view of the district in BS_CA scenario; (b) East façades of Bld_N1 in AS_HA scenario.

Table 10 – Results from the solar analyses on the East façade of Bld_S1.

Scenario	**Entire façade**		**Bottom Floor**				**Top Floor**			
	Irr_{gl} [kW h/(m^2 a)]	Δi	Irr_{gl} [kW h/(m^2 a)]	Δi	$Δi_{cold}$	$Δi_{hot}$	Irr_{gl} [kW h/(m^2 a)]	Δi	$Δi_{cold}$	$Δi_{hot}$
BS_CA	594.8		532.4				647.4			
BS_HA	623.4	+5%	563.1	+5%	+5%	+6%	672.8	+4%	+3%	+4%
AS_CA	598.7	+1%	524.9	-1%	-2%	-1%	658.3	+2%	+1%	+2%
AS_HA	633.9	+6%	561.6	+5%	+4%	+5%	690.2	+6%	+5%	+7%

Irr_{gl}: average annual global solar radiation; Δi: percentage of variation compared to the scenario BS_CA; $Δi_{cold}$: percentage of variation compared to the scenario BS_CA in the cold season (autumn - winter); $Δi_{hot}$: percentage of variation compared to the scenario BS_CA in the hot season (spring - summer)

The solar potential of the East façade is influenced by the variation of height and albedo in the different scenarios. The increment of albedo from 0.5 to 0.95 in scenario BS_HA produces an increase compared to BS_CA of about 5 % on the entire façade (Table 10); the increment is similar at the bottom and at the top floors. Despite the addition of one story on the Bld_S2, the solar potential of the façade of Bld_S1 is constant in the AS_CA scenario and it increases about 6% in the AS_HA scenario. In spite of the high distance from Bld_S2 (Garden H/W = 0.63), the lower floors of Bld_S1 are slightly affected by the shadow caused by the additional story on the Bld_S2. However, with high albedo the global irradiation increases about 5 % compared to BS_CA thanks to the higher reflected radiation. The analysis of the seasonal trends shows that the bottom floor has the higher seasonal increments in the BS_HA scenario (albedo = 0.95), reaching 6 % more than the values in BS_CA (albedo = 0.5) in the hot season. In the cold season, the lower floor is more affected by the shadow of Bld_S2, with losses of 2 % in the AS_CA. The increment of albedo in the AS_HA scenario covers these losses and increases the solar potential of about 4%. The outcomes of the analyses for the top floor show that the solar potential increases in both hot and cold seasons compared to the reference scenario (BS_CA). The highest increment is up to 7% in the hot season for AS_HA with added story and high albedo (Table 11). The solar potential analyses on the façades of Bld_S2 have shown a significant influence of the shadow caused by the surrounding buildings Bld_N2 and Bld_N3. The South façade (Irr_{gl} = 405 kWh/(m^2 a)) is shaded by the presence of Bld_N2, which is three floors higher than the analyzed building, while the solar potential of the East façades is affected by the presence of Bld_N3 (Table 11). The addition of one story does not increase the average annual global solar radiation on the entire façade, while the solar potential on the added story´s façade is 7% higher than the value on the top floor in the baseline scenarios.

Moreover, the façade does not take advantage from the increment of façade's albedo since the materials reflectivity of the nearby building Bld_N3 does not change.

Table 11 – Results from the solar analyses on the East façade of Bld_S2.

Scenario	**Entire façade**		**Bottom Floor**				**Top Floor**			
	Irr_{gl} [kW h/(m^2 a)]	Δi	Irr_{gl} [kW h/(m^2 a)]	Δi	$Δi_{cold}$	$Δi_{hot}$	Irr_{gl} [kW h/(m^2 a)]	Δi	$Δi_{cold}$	$Δi_{hot}$
BS_CA	436.9		364.4				502.8			
AS_HA	436.9	+0%	364.4	+0%	-1%	-1%	541.6	+7%	+1%	+5%

Irr_{gl}: average annual global solar radiation; Δi: percentage of variation compared to the scenario BS_CA; $Δi_{cold}$: percentage of variation compared to the scenario BS_CA in the cold season (autumn - winter); $Δi_{hot}$: percentage of variation compared to the scenario BS_CA in the hot season (spring - summer)

4.1.2. *Solar accessibility of the surrounding buildings*

The analysis of the impact of the optimization interventions applied in Bld_S1 and Bld_S2 was focused on surrounding building Bld_N1 (Table 12), which resulted the most affected by shadowing created by the presence of the Bld_S1 and of a trees' line located along *Via Brescia*. In BS_HA scenario, the increment of albedo from 0.5 to 0.95 improves the solar radiation on the entire East façade (E in Figure 11b) of about 10 %. The increment is similar at the bottom and at the top of the façade, while the addition of one story in AS_CA scenario causes a reduction of solar accessibility about 7 % on the entire surface. The bottom floor (Δi = -5 %) is less affected than the top floor, on which the reduction is almost doubled (Δi = -9 %). The results are explained by the presence of a significant overshadowing effect at the bottom floor already in the baseline scenarios, due to the higher height of Bld_S1 and the proximity of the façade to the trees' line. However, the increase of albedo in the AS_HA scenario counterbalances the losses caused by the additional floor and increases the solar accessibility on the analyzed façade up to 6%. The increment is higher at the bottom floor (Δi = +7 %) than at the top floor (Δi = +5 %).

Table 12 – Results from the solar analyses on the East façade of Bld_N1.

Scenario	**Entire façade**		**Bottom Floor**				**Top Floor**			
	Irr_{gl} [kW h/(m^2 a)]	Δi	Irr_{gl} [kW h/(m^2 a)]	Δi	$Δi_{cold}$	$Δi_{hot}$	Irr_{gl} [kW h/(m^2 a)]	Δi	$Δi_{cold}$	$Δi_{hot}$
BS_CA	405.7		308.7				496.9			
BS_HA	450.6	+10%	341.9	+10%	+10%	+10%	555.4	+11%	+10%	+11%
AS_CA	378.8	-7%	295.2	-5%	-9%	-3%	456.3	-9%	-16%	-7%
AS_HA	431.0	+6%	333.0	+7%	+4%	+8%	525.6	+5%	0%	+7%

Irr_{gl}: average annual global solar radiation; Δi: percentage of variation compared to the scenario BS_CA; $Δi_{cold}$: percentage of variation compared to the scenario BS_CA in the cold season (autumn - winter); $Δi_{hot}$: percentage of variation compared to the scenario BS_CA in the hot season (spring - summer)

The results demonstrate that the reflected radiation due to the increased albedo of Bld_S1 has a significant influence on the solar accessibility of Bld_N1, even if *Via Brescia*´s height to width ratio is low (H/W = 0.85) and the presence of the trees' line separates the two buildings. Furthermore, the seasonal analysis shows that the albedo increment in BS_HA raises the solar accessibility of the entire façade about 10% in both seasons compared to BS_CA. On the contrary, the increment of one story in AS_CA scenario causes higher losses in the cold season. For the bottom floor, the loss is about 9% in the cold season and 3% in the hot season. The upper floor is more influenced, with losses of around 16% in hot season and 7% in cold season. The increment of the albedo to 0.95 in the added story scenario (AS_HA) produces an increase of around 8% in hot season for the bottom floor and 7% for the top floor. During the cold season the increment is more relevant for the bottom floor (Δi = + 4%), while the top floor reaches almost the initial values of the BS_CA scenario. This confirms that the solar accessibility at the lower floors is mostly influenced by the diffuse solar radiation; while, for the upper floors, the reduction of the direct solar radiation due to the additional story has a more relevant effect, which, however, could be completely counterbalanced by the high albedo.

4.2. *Microclimate analysis*

The microclimate analyses run in this study focused (i) on the identification of hot spots, (ii) on the assessment of the impact of the different scenarios above described and (iii) on the mitigation effects provided by green façades.

4.2.1. *Localization of the hot spots and evaluation of human thermal comfort*

The microclimate analysis of the BS_CA scenario shows that the peak of the thermal stress are achieved at 15:00. At this time, the spatial distribution of the meteorological parameters that influence the human energy balance (i.e. T_{air}, T_{mrt}, W_s and RH) and the consequent physiological stress at pedestrian level evaluated with PET, have been assessed for several points of the case study district. The hot spots are localized in the middle of *Via Palermo* and *Via Cagliari* (Figure 12a) where T_{air} reaches 38.4 °C and 38.2 °C respectively; T_{mrt} is higher than 70 °C and PET higher than 45 °C in both the urban canyons (Table 13).

Table 13 – Microclimatic characteristics of significant spots in the canyons with same orientation, i.e., *Via Palermo, Garden, Via Brescia* and *Via Cagliari*.

Urban canyon	**H/W**	**Ground**	**T_{air} [°C]**	**T_s [°C]**	**T_{mrt}[°C]**	**Irr_{SW} [W/m^2]**	**Ws [m/s]**	**PET [°C]**
Via Palermo	0.60	Asphalt	38.36	48.80	71.60	580	0.2	49.1
Garden	0.56	Loamy	36.60	45.20	71.00	570	0.4	46.0
Via Brescia	0.84	Asphalt	36.80	35.60	54.00	110	0.4	38.3
Via Cagliari	0.78	Asphalt	38.13	49.50	72.80	590	1.2	47.2

Other hot spots are localized in the Southern part of *Via Brescia*, at the intersection with *Via Cagliari*, both in the middle and in the proximity of the buildings Bld_S1 and Bld_N2. In the *Garden*, the higher temperatures occur in the Northern part at the corner of Bld_S2, while the lowest values of the entire domain are registered around the Bld_S1. Compared to the *Garden* area, the hot spot in *Via Palermo* is characterized by higher T_{air} and T_s even though T_{mrt} and Irr_{SW} intensity is practically the same despite the different ground material–asphalt in *Via Palermo* and loamy soil in the *Garden*. Compared to *Via Brescia*, *Via Palermo* is characterized by a lower aspect ratio (H/W) and a higher incoming Irr_{SW}, which determine higher values of T_{air}, T_{mrt}, T_s and PET. The hot spot in *Via Cagliari*, shows a reduction of PET of about 2°C compared with the one in *Via Palermo*. Hence, despite having similar T_{air}, T_s, T_{mrt} and Irr_{SW} values and a higher H/W ratio, the conditions in *Via Cagliari* are mitigated by the higher W_s in the urban canyon.

T_{mrt} is one of the most important parameters that influence PET. T_{mrt} includes Irr_{SW} and Irr_{LW} radiation fluxes (both direct and reflected) to which a human body is exposed. *ENVI-met* calculates directly T_{mrt} in two dimensions by taking as input all-sky global radiation, environmental air temperature, vapor pressure, and wind speed and direction [11,70]. Figure 12b shows the spatial correlation between T_{mrt} and Irr_{SW} values during the peak hour [71–73]. Shadowed areas (Irr_{SW} = 0 W/m^2) match those having lower T_{mrt} values, while areas with the highest T_{mrt} correspond to those fully sunlit, which are represented as black dots. With T_{mrt} values above 46 °C in the entire domain, the PET results everywhere above 38 °C, therefore in the grade of physiological strong heat stress (35 °C < PET < 41 °C).

From the analysis of the BS_HA scenario, two major evidences arise. Firstly, a multitude of microclimate conditions exists within a same neighborhood, and even along the same building's façades; this outcome is in accordance with previous studies of Santamouris et al. [74]. In this regard, at the same hour of the day (15:00), the

T_{air} can differ even by 2 °C in different hot spots of the same district. The three urban canyons in *Via Palermo, Via Brescia* and in the *Garden* are quite different from each other: *Via Palermo* is a main road with just few isolated trees; the *Garden* has a strong presence of natural ground (i.e. loamy soil and grass); while *Via Brescia* is a service road highly shadowed by the row of trees alongside it. They also differ in the aspect ratio and shadow pattern. The hot spots are located in the middle of two streets with different orientation, *Via Palermo* and *Via Cagliari*. *Via Palermo* is the warmest area due to the combined effect of maximum incoming Irr_{SW} and minimum W_S on an area with artificial ground material (i.e. asphalt). Indeed, despite the presence of buildings and trees shadows, the Irr_{SW} is not reduced in the hot spot area during the central hours of the day. This aspect, combined with the low W_S due to the district morphology, affects the increase of T_{air}, T_s and T_{mrt}, which are factors that strongly influence the human thermal comfort at pedestrian level (i.e. PET value).

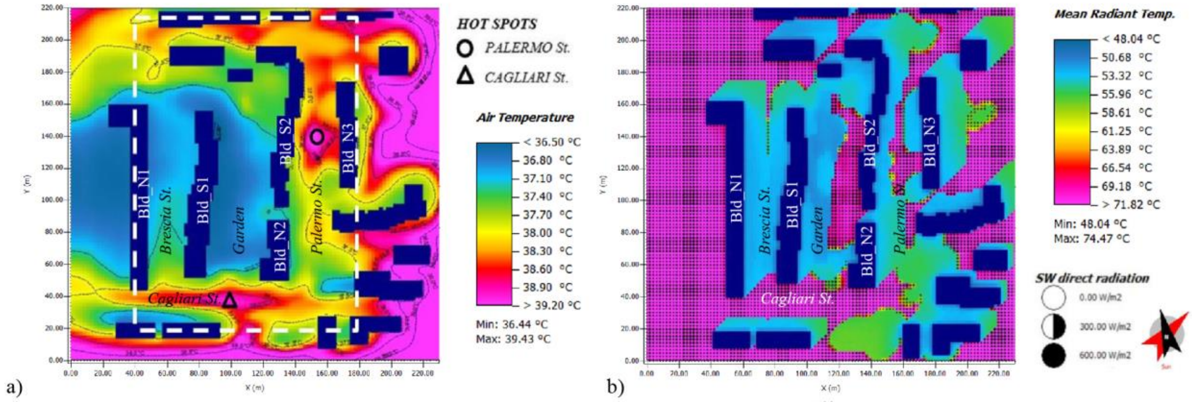

Figure 12 – Spatial distribution of T_{air} (a) and the correlation of spatial distribution between the T_{mrt} and Irr_{SW} (b) at 15:00 at 1 m height from the ground. The visualizations have been generated by Leonardo tool.

Secondly, the temperature during the central hours of the day remains high and thermal stress cannot be reduced in any canyon, despite the presence of aboveground leafy growth in the district and the wide garden in-between the two analyzed buildings. Concerning this evidence, it is reasonable to state that by reducing the vegetation, the district would be hit by even higher temperatures. Indeed, according to Santamouris et al. [74], the low evaporative heat flux in cities is the most significant factor causing the increase of temperatures in urban areas. This is observed to some extent in the *Garden*, where the evapotranspiration from the natural ground (loamy soil and grass) contributes to reduce the T_{air}, T_s and T_{mrt} compared to the other canyons with asphalt.

4.2.2. *Impacts of urban morphology modifications on the microclimate*

The modifications of urban surfaces, which have been tested in the different scenarios, does not provide any significant change on microclimate conditions. Indeed, only T_{air} and T_{mrt} slightly vary, without any relevant consequent improvements on human thermal comfort (PET > 36 °C).

However, some local benefits could be noted. In the configuration with one added story, AS_CA, the maximum value of T_{air} is lowered by almost 1°C and the benefit is confirmed also in the scenario with higher albedo, AS_HA. The T_{mrt} decreases no more than 1.8 °C in both scenarios; such decrement does not improve considerably the PET values compared to the BS_CA scenario. Nevertheless, locally and in proximity to the façades of the building, the T_{air} present some improvements. In the scenarios BS_HA and AS_HA, the distribution of T_{air} was analyzed on the film layer adjacent to the East and West façades of building Bld_S2 (Figure 13) registering a reduction of 0.7 °C. This is caused by the high albedo finishing material on the building façade as demonstrated in several studies in literature [75,76].

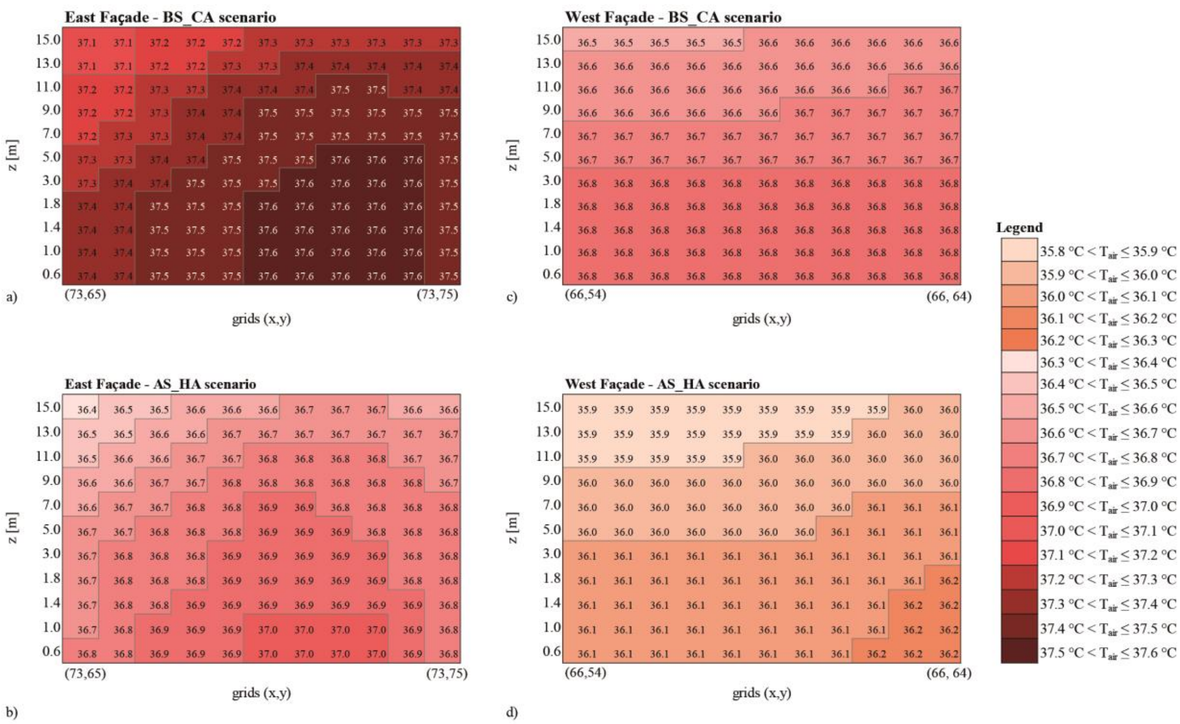

Figure 13 – Comparison between BS_CA and AS_HA scenarios of T_{air} distribution on film layer of East (a,b) and West (c,d) façades of Bld_S2.

4.2.3. *Impacts of green façade installation on microclimate*

On the building Bld_S2, the installation of the green façade has been evaluated as further potential design intervention. The outcomes of the microclimate analyses show that the presence of the green façade allows to reduce of about 0.3 °C the T_{air} at the adjacent layer of the analyzed façade, and up to 0.5 °C the T_{air} at the hot spot in *Via Palermo* (Figure 14). With regard to thermal comfort conditions, PET in the hot spot is decreased of 0.8 °C, from 49.1 °C in the baseline scenario BS_CA to 48.3 °C in the Gr_Fac one, although the level of thermal stress on the human body remains in the grade of physiological extreme heat stress (PET > 41 °C).

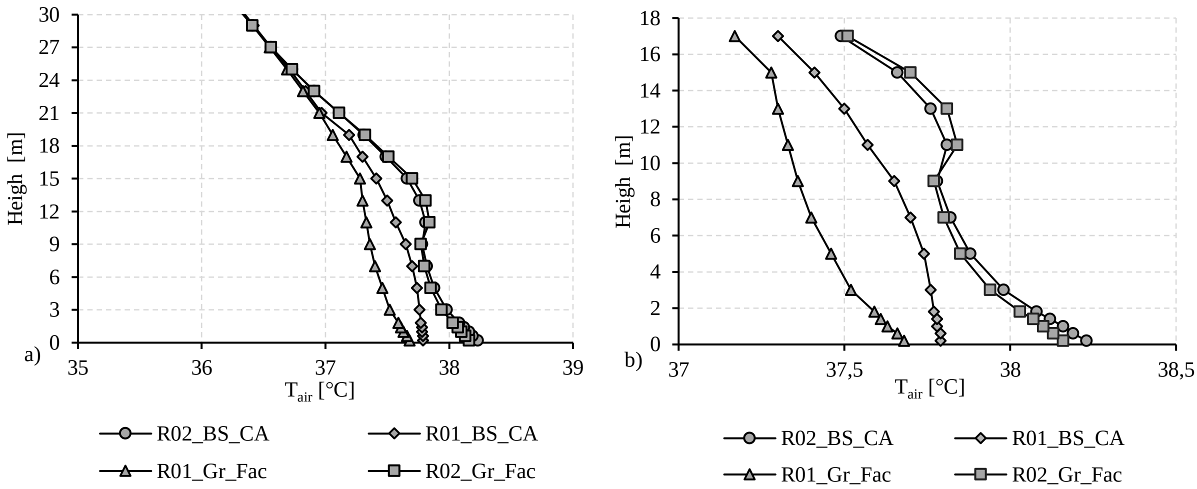

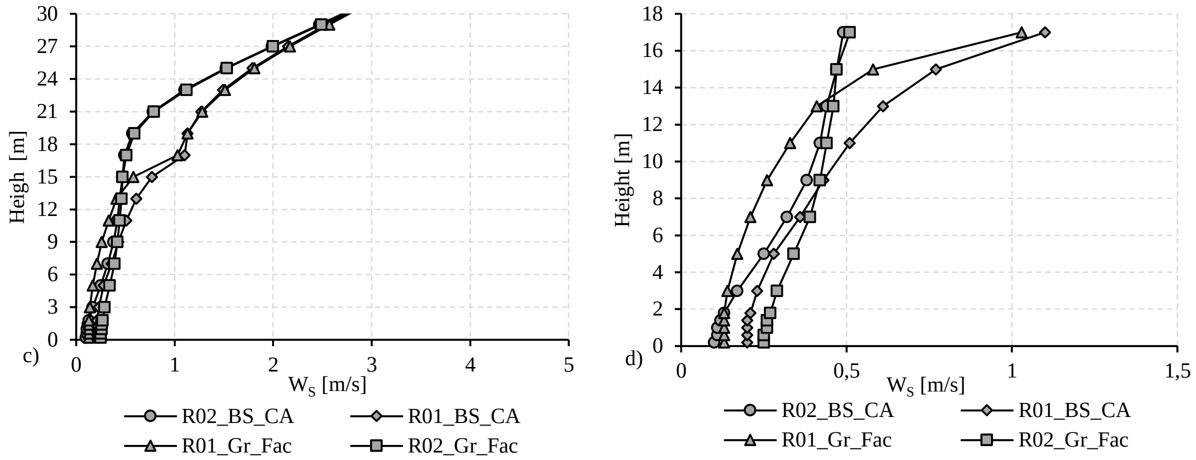

Figure 14 – Trend of T_{air} (a) along the entire domain and (b) for the height of the façades, and W_S (c) at R01 along the film layer adjacent of the analyzed façade of Bld_S2 and (d) at R02 in proximity of the hot spot in *Via Palermo* in BS-CA and Gr_Fac scenarios.

The trend of the T_{air} varies along the height of the façade (data from receptor R01 positioned at the bottom of the façade). The highest reduction is registered in the middle, while, on the bottom and top, the benefit given by the presence of the green is almost negligible (Figure 14b). Furthermore, the presence of the vertical greening halves the intensity of the W_S in the bottom and central part of the façade (Figure 14 c and d). Almost no benefits have been observed, due to the presence of the green façade, at receptor R02, which is positioned at the hot spot in *Via Palermo*. These findings are quite aligned to the outcomes of similar studies in literature [77–83] and the small effect strongly depends on the low density of the chosen foliage of the trees' crown. Still, given the local benefits in terms of air temperature mitigation and consequently on thermal stress at pedestrian level, the installation of the green façade has been taken into account for the first floors of the Bld_S1.

4.3. *Urban airflow analysis*

In this study, CFD analyses at urban scale were conducted in order to study the ventilation effect given by the airflow conditions in proximity to the East façades of both buildings Bld_S1 and Bld_S2 for assessing the effectiveness of a technological solution consisting of a DSF coupled with BiPV (AS_DSF_BIPV scenario).

4.3.1. *Assessment of ventilation effect for the installation of a double skin façades*

In the scenario BS (Figure 15a), the wind speed in proximity to the façade varies from 1 m/s at the bottom floor to 2.5 m/s in the upper part of the façade of Bld_S1. With the addition of one story (i.e. AS scenario), the wind speed increases to values greater than 2 m/s along almost the entire façade and reaches 3.5 m/s on the top floor and on the roof (Figure 15b). This is explained by the fact that adding one story, Bld_S1 becomes higher than Bld_N2 and, hence, the influence of the nearby buildings is reduced in the upper part of the building causing an increase of the wind speed. Furthermore, the wind flow is quite perpendicular to the façade and the wind shadow caused by Bld_N2 and Bld_S2 has only a moderate influence. In AS_DSF_BIPV scenario, the wind speed in the cavity of the double-skin façade is around 1.5 m/s on almost the entire height of the building and increases to 2.5 m/s on the upper part of the façade, which was the area defined for installing BIPV from the previous analysis described in Section 4.1.1 (Figure 15c). As demonstrated in previous studies [84–86], the reached intensity of the wind speed through the cavity is suitable to reduce the operative temperature of the solar system and increase the efficiency and the durability of the PV modules [87,88]. An additional benefit provided by this solutions was already proved by Mirzaei [85] who demonstrated that the presence of an air cavity behind the PV can decrease the mean surface temperature of around 8 °C and the maximum surface temperature of more than 10 °C for wind velocities around 2 m/s and incident radiation of 200 kWh/(m^2 a).

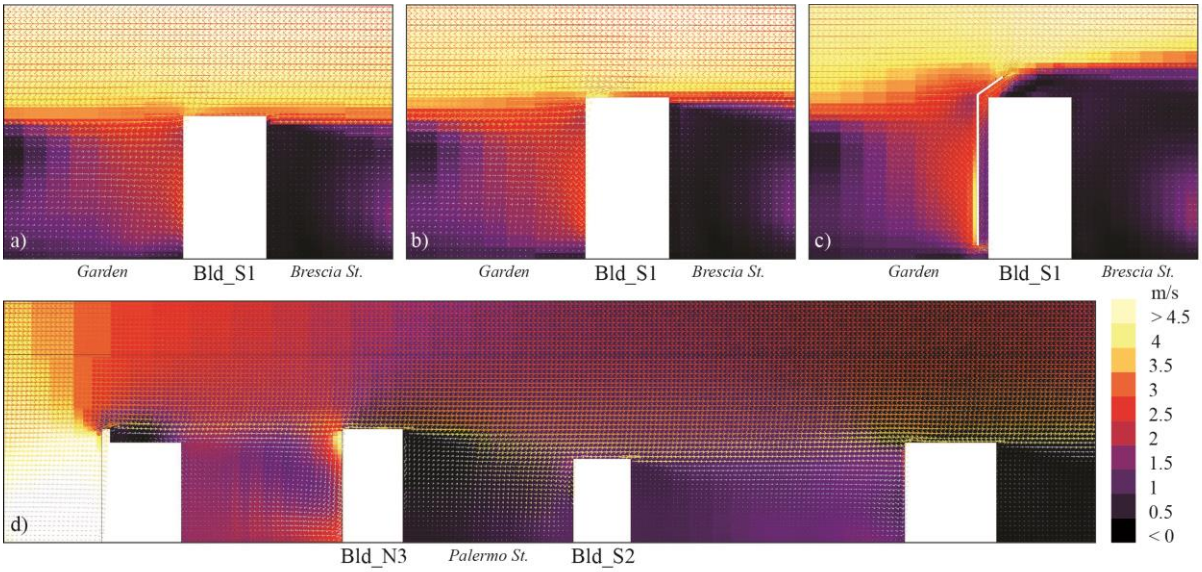

Figure 15 – Wind speed profile resulting from the CFD analyses. In the section AA' (Figure 10) (a) Building Bld_S1 - Scenario BS; (b) Building Bld_S1 - Scenario AS; in the section BB'(Figure 10) (c) Building Bld_S1 - Scenario AS_DSF; (d) Building Bld_S2 - Scenario AS.

A CFD analysis was conducted for Bld_S2 in order to define whether the wind speed and direction in proximity to the East façade are convenient for installing a DSF (Figure 15d). The wind speed up to the first half of the façade (i.e. lower three floors) is around 1 m/s and decreases to about 0.5 m/s on the fourth and fifth floor, as a result of the shadow caused by Bld_N3. On the top floor and the roof, the wind velocity reaches values around 1.5 m/s. Furthermore, the prevalent direction of the airflow is not perpendicular but quite parallel to the façade, due do the presence of the urban canyon of *Via Palermo* that channel the wind flow along its direction without providing any advantage to the analyzed façade. For all these reasons, Bld_S2 was not considered suitable for installing a DSF and the roof was maintained flat.

4.4. *Solar potential analyses to assess the installation of BIPV systems on double skin façade*

The last set of simulations was conducted on the surfaces of the DSFs, in the configuration resulted from the CFD analysis, in order to estimate the suitability of solar systems installation, such as the integration of PV panels. The maximum levels of global solar radiation have been calculated for (i) horizontal surfaces and (ii) surfaces with optimal tilt (38° from the horizontal) and azimuth (7.5° West) (Table 14). The solar potential of the tilted surfaces of Bld_S1 resulted 12% lower than the corresponding maximum value for tilted angle and azimuth. The reason for this significant reduction is twofold: (i) the azimuth of the building (8° E) is rotated 15.5° compared to the optimal one (7.5° W), and (ii) the incoming solar radiation is influenced by the complex overshadowing effects due to the presence of the surrounding buildings. However, the solar potential of the tilted surfaces is higher than the horizontal ones; therefore, those surfaces are more suitable for the installation of solar systems than the flat roof, which has been considered in the added story scenarios. The upper part of the vertical façade (i.e. from fifth floor up) results also suitable for installing solar systems with average Irr_{gl} values of around 600 kW h/(m^2 a). With regard to Bld_S2, solar analyses were conducted for two different configurations. Initially, the solar potential of East façade surfaces with optimal tilt was estimated. In this configuration, the average Irr_{gl} resulted 21% lower than the maximum solar radiation for unobstructed surfaces with optimal tilt and azimuth.

Table 14 – Solar analyses on the surfaces of the DSFs of Bld_S1 and Bld_S2.

Object	**Surface description**	**Irr_{gl} [kW h/(m^2 a)]**	**Δi**
Maximum values on a surface	Horizontal surface*	1046	
	Surface with optimal tilt (38 ° from horizontal) and azimuth (7.5 West) *	1173	
Values on the roof of Bld_S1	Bld_S1 - Roof with optimal tilt (38 ° from horizontal)	1047	-12%
Values on the roof of the Bld_S2	Bld_S2 - Roof with optimal tilt (38 ° from horizontal)	970	-21%
	Bld_S2 - Flat Roof	1017	-3%

Irr_{gl}: average annual global solar radiation; Δi: percentage of variation compared to the reference maximum values

* Solar radiation calculated on unobstructed surfaces with optimal azimuth and tilt

In the second configuration, the Irr_{gl} of the flat roof was estimated equal to 1017 kW h/(m^2 a). This value is 3% lower than the maximum Irr_{gl} for an unobstructed horizontal surface (Table 14). The results obtained in the previous steps of the study already highlighted the low solar radiation levels (section 4.1) and the poor airflow in the proximity of the building (section 4.3). Therefore, the findings from these further solar potential analyses confirm the inconvenience to install a double-skin façade for Bld_S2, while the horizontal surface of the roof has adequate solar radiation (Irr_{gl} higher than 1000 kW h/(m^2 a)) for installing solar systems.

4.5. *Final configuration of the design and technological interventions to optimize the use of the buildings' surfaces to exploit RES*

The conducted analyses have provided clear indications on the design and technological interventions that might be applied in the case study district. From the solar analyses (Section 4.1 and 4.4), the most suitable surfaces to install solar systems (highlighted in dashed line in Figure 16a) have been identified.

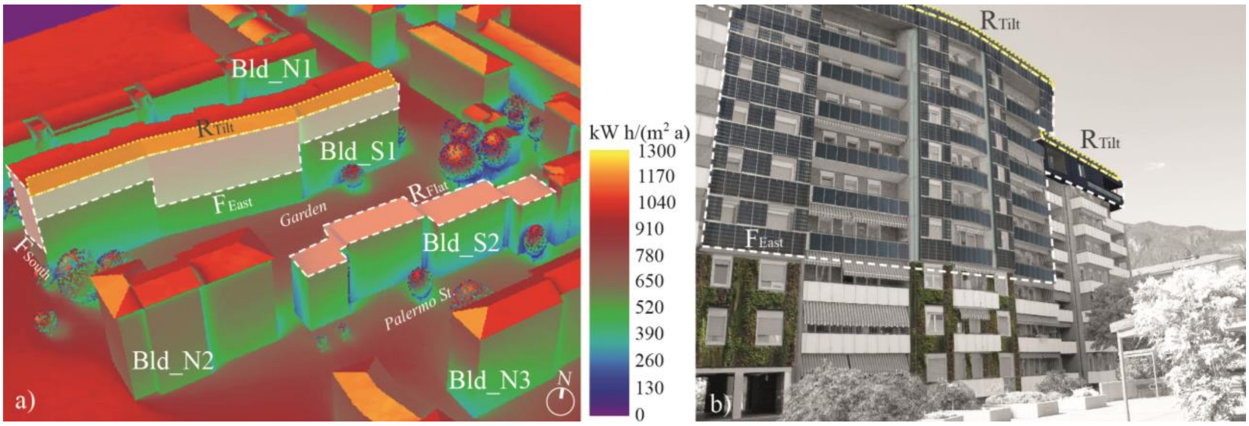

Figure 16 – (a) Identification of the surfaces suitable for installing solar systems in the final optimized scenario. (b) Visualization of the final design interventions on the façade of Bld_S1 in the scenario with one added story volume: green façade on the first three floors and DSF system coupled with BIPV from the fourth floor.

When designing the installation of solar systems on the façades of the Bld_S1, only the upper floors (i.e. from fourth floor up to R_{Tilt} in Figure 16a) should be considered in order to avoid both the overshadowing effect from the surrounding buildings on the bottom floors and any eventual impact of the systems in increasing the T_s and outdoor T_{air}, with consequently effect on the thermal stress at pedestrian level. In that regard, in order to exploit the local benefits in terms of air temperature's reduction, the green façade should be installed on the first floors (Figure 16b), while the DSF system should be inserted from the fourth floor up, in order to avoid the wind shadow caused by the buildings in front (i.e. Bld_S1 and Bld_N2). The conducted analyses have also demonstrated that, for Bld_S2, different design interventions should be applied. For example, high albedo materials should be used on the façades in order to increase the solar radiation reflection that allows to counterbalance the overshadowing effect created by Bld_S1, as demonstrated by the conducted solar analyses. The same design intervention should be applied on the Northern side of Bld_S1 in order to counterbalance the overshadowing effect created on Bld_N1. Finally, on Bld_S2, solar active systems such as PV or ST should be installed on the flat roof (R_{Flat} in Figure 16a), which is the most radiated surface.

5. Limitations of the study

This section presents some limitations of the study that might represent its possible future developments. Firstly, the energy production from solar systems has not been estimated in this study given that its main focus is related to demonstrate the application of the proposed holistic approach in the early design phases to assess the exploitation of RES for bioclimatic strategies as well as design and technological interventions. The calculation of energy production derived from the PV and ST panels might be conducted in a further phase of the design process, when all the design choices have been taken. In that regard, more accurate software such as *PVsyst* and/or *Polysun*, which calculate the energy production not only using the efficiency of the systems, but also considering all energy losses of the plant components and the grid, should be used. Good et al. [9] demonstrated that, by combining modelling design tools (i.e. *Rhinoceros* and *Grasshopper*) with dynamic solar simulation software (i.e. *DIVA-for-Rhino*, *Radiance* etc.) and dedicated tools for energy outputs estimation (i.e. *PVsyst* and/or *Polysun*), a thorough and precise calculation of the energy production from solar systems could be reached. In this way, all the critical aspects, from overshadowing effect and solar reflections, to the energy losses from the systems and the grid can be taken into account. Furthermore, a future development of the study in terms of solar accessibility might include analyses of indoor and outdoor daylight at ground level, given its significant influence on the users' perceived visual comfort in and around the buildings, as well as on the energy consumption of the buildings.

Secondly, in relation to the microclimate analysis, some remarks on the results presented in this study are worth to be observed. The model outputs strongly depend on the quality of the data used to force the model. For this study, the input climatic data (i.e. T_{air}, RH, average W_S, and prevalent wind direction) were not collected directly on site, as this was not possible at the time of the investigation, but from a weather station located on the city hospital roof, at a distance of about 1700 m North-West from the neighborhood site. Furthermore, some other uncertainties must be considered in relation to T_{air}, T_S, T_{mrt}, and Irr_{SW}, which can suffer from overestimation due to the following reasons:

- The model does not account for possible positive effects caused by local increments of wind speed at street level. Indeed, *ENVI-met* computes the W_S starting from the mean value measured at 10 m height, but the turbulence in a street canyon is normally higher than at higher levels [42], and hence might favorite a local reduction of T_{air}.
- *ENVI-met* does not allow taking into account the shadow given by far objects such as the mountains. In this regard, it has to be observed that the critical location of the district within the city of Bolzano, which is located in a valley surrounded by mountains, could have relevant impact on the total incoming Irr_{SW}.
- *ENVI-met* cannot simulate moving water systems like rivers and fountains [11]. Therefore, the evaporative cooling effect of the river on the Southern part of the case study district cannot be analyzed, thus contributing to overestimate the T_{air} and PET [72].

- On the other hand, the overestimation due to reasons above explained might be counterbalanced by the impossibility to take into account the anthropogenic heat from both cooling systems [12] and traffic during most critical periods.
- Modelling the green façade in *ENVI-met* resulted quite difficult due to the lack of a specific function in the program. This aspect was overcome by creating an own solution, which presents some limitations in terms of modeling and elements' properties.

Regarding the methodology adopted for the CFD analyses conducted in this study, the limited computational power of the workstation used for running the simulations (Intel Core i7-4720HQ @ 2.60GHz, 8 GB RAM) forced the authors to adopt some simplifications in the model. The presence of trees and vegetation has not been considered due to difficulties in creating the related meshes with the aim of not increasing excessively the computational time. However, several studies demonstrated the relevant influence of urban greenery on the airflow in urban areas [89]. Furthermore, the dimensions of the computational domain were reduced in comparison to the one recommended as best practice for CFD analyses of urban areas [90,91].

Finally, the effect on the indoor thermal conditions of finishing materials installed on the building envelope should be deeper analyzed. As resulted from several studies, the application of "cool materials" (i.e. materials with high solar reflectance) on the building envelope produces benefits in terms of indoor thermal comfort [92,93]. Advantages are registered also on energy savings by decreasing the heat flow entering the building [93] as well as reducing the cooling loads in air-conditioned buildings and by increasing comfort in free-running buildings. Furthermore, the application of cool materials could also provide benefits on thermal heat stress and reduction of global warming [94].

The future developments of the study will focus to address all these limitations.

6. Conclusions

The main purpose of the study was to develop and test a holistic approach of environmental analyses for optimizing the use of urban surfaces at district level. The adoption of the proposed methodology, in which several environmental parameters were considered, and different numerical models were used, led to the optimized identification of potential design interventions in term of (i) solar active and passive strategies, (ii) outdoor microclimate and thermal comfort, and (iii) ventilation strategies. The findings of the study have both practice and policy implications.

6.1. *Practical implications*

The preliminary analysis of the climate of the city demonstrates the importance of taking into consideration multiple climatic factors already before, and during the actual early design phase, to propose bioclimatic strategies, and to make the best use of the RES potentiality at district scale.

The solar analyses have demonstrated the important role played by urban morphology characteristics, such as aspect ratio of urban canyon, and building envelope characteristics, such as finishing materials of the façades, when enhancing solar accessibility and solar potential at district scale. The analyses provided evidence that:

- As demonstrated in previous studies [95], preliminary 2D and/or 3D sun path and solar potential analyses on a building or group of buildings located in a complex built environment are an essential support instrument to study the impact of the urban surrounding in terms of solar accessibility and overshadowing effect [96,97]. Early stage analyses allow to localize the most suitable areas for solar systems installation on the buildings' envelope and to minimize the losses given by urban compactness and high density of the existing urban areas, especially in the case of refurbishment interventions [98].

- The shadowing on the surrounding buildings, caused by the addition of one story, can be compensated by an increase of the building surfaces albedo.
- The added story, being usually unshaded, is suitable for installing active solar systems and therefore can strongly contribute to the overall efficiency of the district through the production of solar energy, which can cover a quite consistent amount of the total energy needs.
- When designing solar systems with the objective to maximize the solar potential, it is not sufficient to consider only the optimal tilt angle of the surfaces on which they are installed. The azimuth of the systems and the characteristics of the surrounding environment (e.g., buildings and trees creating overshadowing) also have a great influence and should be taken into account.

In terms of microclimate conditions, the major evidences emerged are:

- A passive solution such as the change of finishing materials' albedo does not consistently modify the climate parameters of air temperature, surface temperature, and mean radiant temperature in the urban canyons. Instead, the increment of the height of the buildings reduces the air temperature in the urban canyons at street level and along the film layer close to the façades.
- Thermal comfort cannot be easily achieved during a typical hot summer day in a continental climate city [99].
- The air temperature at street level tends to increase when high albedo materials are employed, although the increment is negligible. Instead, the air temperature decreases slightly by incrementing the height of buildings due to the consequent increase of the aspect ratio of the urban canyon. This fact reduces the sun exposure of the hot spot areas during the warmest hours of the day

The combination of solar analyses with CFD simulations plays a key role in the design of DSFs and BIPV systems. The results from these analyses highlight the following aspects:

- The airflow in complex urban environment could be channeled in urban canyons and create turbulences and prevalent wind directions suitable to activate active and passive strategies at building and district scales.
- Conducing ventilation analyses in the preliminary phases of the design process allows to define the optimal location and geometry of the façade, and to guarantee a level of airflow on the back of the PV modules suitable to reduce their surface temperatures, hence increasing their efficiency and durability [87,88].
- The aspect ratio of the urban canyons, the finishing materials of the façades, and the design of the building envelope in terms of ventilation strategies and green solutions are key aspects that designers and municipalities should take into account before and during the early planning phases of design interventions.

Finally, a further development of the presented study might be the economic evaluation for the proposed design interventions. An interesting progress of the research might be the quantification of the investment costs for the installation of solar active systems, double-skin and green façades in order to estimate the economic feasibility of the interventions by assessing, for example, the payback time of the interventions.

6.2. *Policy implications*

The proposed approach could be successfully employed to optimize the use of urban surfaces to enhance climatic-driven building design interventions and their impact on the microclimate of existing neighborhoods. Buildings can be considered as “climate modifiers” which should be shaped to take advantage of local weather to enhance their architectural integrity and environmental quality [100], and to improve outdoor microclimate conditions in their surroundings. Therefore, the numerical assessment combining environmental and numerical analyses is helpful to improve the design interventions before the definitive stage. In this way, it is possible to consider both climate boundary conditions and outdoor impact of retrofit solutions, and to take effective design decision in the early design stages when adjustments are still possible. Furthermore, this work could be successfully used to establish a constructive dialog between urban planners, designers and researchers in order to develop design guidelines and urban planning recommendations to prioritize design interventions in existing urban areas aimed at optimizing the use of urban surfaces. Finally, the produced energy on site could cover part of the energy demand of the district in order to initiate a transition towards a self-sustainable urban district. This may become a good practice for the Italian municipalities and construction decision makers, especially because interventions of building refurbishment and urban renewal will become very common due to the age of a relevant part of the Italian building stocks.

Acknowledgements

The research leading to these results has received funding from the European Union’s Seventh Programme for research, technological development and demonstration under grant agreement No. 609019. The European Union is not liable for any use that may be made of the information contained in this document, which is merely representing the authors view. The authors are grateful to Bartolomeo Ventura (European Academy of Bolzano) for the climatic datasets of the weather stations.

References

[1] L. Laski, S. Schellekens, Growing Up Urban: State of World Population 2007, State World Popul. 2007 Youth Suppl. (2007). doi:10.1111/j.1540-5931.2007.00426.x.

[2] United Nations - Department of Economic and Social Affairs - Population Division, World Population Prospects: The 2015 Revision, Key Findings and Advance Tables, (2015). doi:10.1017/CBO9781107415324.004.

[3] P. Moonen, T. Defraeye, V. Dorer, B. Blocken, J. Carmeliet, Urban Physics: Effect of the micro-climate on comfort, health and energy demand, Front. Archit. Res. 1 (2012) 197–228. doi:10.1016/j.foar.2012.05.002.

[4] N. Gaitani, M. Santamouris, C. Cartalis, I. Pappas, F. Xyrafi, E. Mastrapostoli, P. Karahaliou, C. Efthymiou, Microclimatic analysis as a prerequisite for sustainable urbanisation: Application for an urban regeneration project for a medium size city in the greater urban agglomeration of Athens, Greece, Sustain. Cities Soc. 13 (2014) 230–236. doi:10.1016/j.scs.2014.02.006.

[5] M.K.-A. Neophytou, P. Fokaides, I. Panagiotou, I. Ioannou, M. Petrou, M. Sandberg, H. Wigo, E. Linden, E. Batchvarova, P. Videnov, B. Dimitroff, A. Ivanov, Towards Optimization of Urban Planning and Architectural Parameters for Energy use Minimization in Mediterranean Cities, World Renew. Energy Congr. (2011).

[6] A. Kalua, Envelope Thermal Design Optimization for Urban Residential Buildings in Malawi, Buildings. 6 (2016) 13. doi:10.3390/buildings6020013.

[7] M. Kolokotroni, I. Giannitsaris, R. Watkins, The effect of the London urban heat island on building summer cooling demand and night ventilation strategies, Sol. Energy. 80 (2006) 383–392. doi:10.1016/j.solener.2005.03.010.

[8] G. Lobaccaro, F. Fiorito, G. Masera, T. Poli, District geometry simulation: A study for the optimization of solar facades in urban canopy layers, Energy Procedia. 30 (2012) 1163–1172. doi:10.1016/j.egypro.2012.11.129.

[9] C.S. Good, G. Lobaccaro, S. Hårklau, Optimization of Solar Energy Potential for Buildings in Urban Areas – A Norwegian Case Study, Energy Procedia. 58 (2014) 166–171. doi:10.1016/j.egypro.2014.10.424.

[10] E. Bozonnet, M. Musy, I. Calmet, F. Rodriguez, Modeling methods to assess urban fluxes and heat island mitigation

measures from street to city scale, Int. J. Low-Carbon Technol. 10 (2015) 62–77. doi:10.1093/ijlct/ctt049.

[11] M. Bruse, H. Fleer, Simulating surface–plant–air interactions inside urban environments with a three dimensional numerical model, Environ. Model. Softw. 13 (1998) 373–384. doi:10.1016/S1364-8152(98)00042-5.

[12] A. Gros, E. Bozonnet, C. Inard, Cool materials impact at district scale—Coupling building energy and microclimate models, Sustain. Cities Soc. 13 (2014) 254–266. doi:10.1016/j.scs.2014.02.002.

[13] J. Allegrini, K. Orehounig, G. Mavromatidis, F. Ruesch, V. Dorer, R. Evins, A review of modelling approaches and tools for the simulation of district-scale energy systems, Renew. Sustain. Energy Rev. 52 (2015) 1391–1404. doi:10.1016/j.rser.2015.07.123.

[14] M. Tsitoura, M. Michailidou, T. Tsoutsos, A bioclimatic outdoor design tool in urban open space design, Energy Build. 153 (2017) 368–381. doi:10.1016/j.enbuild.2017.07.079.

[15] M. Shahrestani, R. Yao, Z. Luo, E. Turkbeyler, H. Davies, A field study of urban microclimates in London, Renew. Energy. 73 (2015) 3–9. doi:10.1016/j.renene.2014.05.061.

[16] A. Macleod, Using the microclimate to optimise renewable energy installations, Renew. Energy. 33 (2008) 1804–1813. doi:10.1016/j.renene.2007.10.010.

[17] European Climate Foundation, Roadmap 2050 project, (n.d.). http://www.roadmap2050.eu/ (accessed November 16, 2015).

[18] J. Kanters, M. Wall, A planning process map for solar buildings in urban environments, Renew. Sustain. Energy Rev. 57 (2016) 173–185. doi:10.1016/j.rser.2015.12.073.

[19] G. Lobaccaro, S. Carlucci, S. Croce, R. Paparella, L. Finocchiaro, Boosting solar accessibility and potential of urban districts in the Nordic climate: A case study in Trondheim, Sol. Energy. 149 (2017) 347–369. doi:10.1016/j.solener.2017.04.015.

[20] M. Kottek, J. Grieser, C. Beck, B. Rudolf, F. Rubel, World map of the Köppen-Geiger climate classification updated, Meteorol. Zeitschrift. 15 (2006) 259–263. doi:10.1127/0941-2948/2006/0130.

[21] M. Papathoma-köhle, T. Ulbrich, M. Keiler, L. Pedoth, R. Totschnig, T. Glade, S. Schneiderbauer, U. Eidswig, Vulnerability to Heat Waves , Floods , and Landslides in Mountainous Terrain : Test Cases in South Tyrol, Elsevier Inc., 2014. doi:10.1016/B978-0-12-410528-7.00008-4.

[22] Autonomous Province of Bolzano, Meteorological Service of the Autonomous Province of Bolzano - Historical Data, (2017). http://www.provincia.bz.it/meteo/dati-storici.asp (accessed May 20, 2017).

[23] US Department of Energy, Weather Data, (EnergyPlus U.S. Dep. Energy's Build. Technol. Off. - Natl. Renew. Energy Lab. (2016). https://energyplus.net/weather (accessed June 15, 2017).

[24] Municipality of Bolzano, SitSun Project, (2012). http://sit.comune.bolzano.it/SitSun/ (accessed May 20, 2017).

[25] Municipality of Bolzano, Eurac Research, Sustainable Energy Action Plan, (2014).

[26] SINFONIA, Sinfonia. Low Carbon Cities for Better Living., (n.d.). www.sinfonia-smartcities.eu.

[27] Autonomous Province of Bolzano, DGP 5th August 2014 - Implementing directive of the "Bonus Energia," (2014).

[28] M. Milne, R. Liggett, R. Al-Shaali, Climate Consultant 3.0: a tool for visualizing building energy implications of climates, Proc. Sol. Conf. (2007). http://www.energy-design-tools.aud.ucla.edu/papers/ASES07-CC.pdf.

[29] UCLA Energy Design Tools Group, Climate Consultant V6.0, (2014).

[30] M. Sadeghipour Roudsari, Ladybug tools, (2016). http://www.ladybug.tools.

[31] A. Mostapha Sadeghipour Roudsari, Michelle Pak, Smith, Ladybug: a Parametric Environmental Plugin for Grasshopper To Help Designers Create an Environmentally-Conscious Design, 13th Conf. Int. Build. Perform. Simul. Assoc. (2013) 3129–3135. http://www.ibpsa.org/proceedings/bs2013/p_2499.pdf.

[32] McNeel Robert and Associates, Rhino Version 5.0, (2015).

[33] S. Davidson, Grasshopper: Algorithmic Modelling for Rhino, (2014). http://www.grasshopper3d.com/.

[34] I.G. Capeluto, B. Plotnikov, A method for the generation of climate-based, context-dependent parametric solar envelopes, Archit. Sci. Rev. (2017) 1–13. doi:10.1080/00038628.2017.1331334.

[35] S. Carlucci, G. Lobaccaro, Y. Li, E. Catto Lucchino, R. Ramaci, The effect of spatial and temporal randomness of stochastically generated occupancy schedules on the energy performance of a multiresidential building, Energy Build. 127 (2016) 279–300. doi:10.1016/j.enbuild.2016.05.023.

[36] A. McNeil, E.S. Lee, A validation of the Radiance three-phase simulation method for modelling annual daylight performance of optically complex fenestration systems, J. Build. Perform. Simul. 6 (2012) 24–37. doi:10.1080/19401493.2012.671852.

[37] D. Ibarra, C.F. Reinhart, Solar availability: A comparison study of six irradiation distribution methods, Proc. Build. Simul. 2011 12th Conf. Int. Build. Perform. Simul. Assoc. (2011) 2627–2634. http://www.scopus.com/inward/record.url?eid=2-s2.0-84870176731&partnerID=tZOtx3y1.

[38] J. Mardaljevic, Simulation of annual daylighting profiles for internal illuminance, Light. Res. Technol. 32 (2000) 111–118. doi:10.1177/096032710003200302.

[39] C.F. Reinhart, J. Wienold, The daylighting dashboard - A simulation-based design analysis for daylit spaces, Build. Environ. 46 (2011) 386–396. doi:10.1016/j.buildenv.2010.08.001.

[40] G. Ward, The RADIANCE 4.2 Synthetic Imaging System, (2014). http://radsite.lbl.gov/radiance/refer/ray.html (accessed March 14, 2016).

[41] E. Enríquez, V. Fuertes, M.J. Cabrera, J. Seores, D. Muñoz, J.F. Fernández, New strategy to mitigate urban heat island effect: Energy saving by combining high albedo and low thermal diffusivity in glass ceramic materials, Sol. Energy. 149 (2017) 114–124. doi:10.1016/j.solener.2017.04.011.

[42] S. Huttner, Further development and application of the 3D microclimate simulation ENVI-met, (2012).

[43] X. Yang, L. Zhao, M. Bruse, Q. Meng, Evaluation of a microclimate model for predicting the thermal behavior of different ground surfaces, Build. Environ. 60 (2013) 93–104. doi:10.1016/j.buildenv.2012.11.008.

[44] A. Forouzandeh, Numerical modeling validation for the microclimate thermal condition of semi-closed courtyard spaces between buildings, Sustain. Cities Soc. 36 (2018) 327–345. doi:10.1016/j.scs.2017.07.025.

[45] S. Tsoka, K. Tsikaloudaki, T. Theodosiou, Urban space's morphology and microclimatic analysis: A study for a typical urban district in the Mediterranean city of Thessaloniki, Greece, Energy Build. 156 (2017) 96–108. doi:10.1016/j.enbuild.2017.09.066.

[46] F. Salata, I. Golasi, R. de Lieto Vollaro, A. de Lieto Vollaro, Urban microclimate and outdoor thermal comfort. A proper procedure to fit ENVI-met simulation outputs to experimental data, Sustain. Cities Soc. 26 (2016) 318–343. doi:10.1016/j.scs.2016.07.005.

[47] H. Lee, H. Mayer, L. Chen, Contribution of trees and grasslands to the mitigation of human heat stress in a residential district of Freiburg, Southwest Germany, Landsc. Urban Plan. 148 (2016) 37–50. doi:10.1016/j.landurbplan.2015.12.004.

[48] C.S. Gusson, D.H.S. Duarte, Effects of Built Density and Urban Morphology on Urban Microclimate - Calibration of the Model ENVI-met V4 for the Subtropical Sao Paulo, Brazil, Procedia Eng. 169 (2016) 2–10. doi:10.1016/j.proeng.2016.10.001.

[49] J.A. Acero, K. Herranz-Pascual, A comparison of thermal comfort conditions in four urban spaces by means of measurements and modelling techniques, Build. Environ. 93 (2015) 245–257. doi:10.1016/j.buildenv.2015.06.028.

[50] CTI, UNI/TS 11300- Technical Standards Reference on savings and energy certification of buildings, (2016). http://11300.cti2000.it/.

[51] M. Bruse, ENVI-met 4: A Microscale Urban Climate Model, (2015). www.envi-met.info.

[52] G. Lobaccaro, J.A. Acero, Comparative analysis of green actions to improve outdoor thermal comfort inside typical urban street canyons, Urban Clim. 14 (2015) 251–267. doi:10.1016/j.uclim.2015.10.002.

[53] F. Olivieri, P. Vidal, R. Guerra, M. Chanampa, J. García, C. Bedoya, Green façades for urban comfort improvement : Implementation in a extreme continental mediterranean climate, Proc. - 28th Int. PLEA Conf. Sustain. Archit. + Urban Des. Oppor. Limits Needs - Towar. an Environ. Responsible Archit. PLEA 2012. (2012). https://www.scopus.com/inward/record.uri?eid=2-s2.0-84886773306&partnerID=40&md5=ae1f32b1df7910b538eff3d0dd20c907.

[54] B. Jänicke, F. Meier, M.-T. Hoelscher, D. Scherer, Evaluating the Effects of Façade Greening on Human Bioclimate in a Complex Urban Environment, Adv. Meteorol. 2015 (2015) 1–15. doi:10.1155/2015/747259.

[55] T. Zölch, J. Maderspachera, C. Wamslerb, S. Pauleit, Using green infrastructure for urban climate-proofing: An evaluation of heat mitigation measures at the micro-scale, Urban For. Urban Green. 20 (2016) 305–316.

[56] P. Höppe, The physiological equivalent temperature - a universal index for the biometeorological assessment of the thermal environment, Int. J. Biometeorol. 43 (1999) 71–75. doi:10.1007/s004840050118.

[57] A. Matzarakis, H. Mayer, M.G. Iziomon, Applications of a universal thermal index: physiological equivalent temperature., Int. J. Biometeorol. 43 (1999) 76–84. doi:10.1007/s004840050119.

[58] H. Mayer, P. Höppe, Thermal comfort of man in different urban environments, Theor. Appl. Climatol. 38 (1987) 43–49. doi:10.1007/BF00866252.

[59] P.. Hoppe, Heat balance modelling, Experimentia. 49 (1993) 741–746.

[60] O. Potchter, P. Cohen, T.P. Lin, A. Matzarakis, Outdoor human thermal perception in various climates: A comprehensive review of approaches, methods and quantification, Sci. Total Environ. 631–632 (2018) 390–406. doi:10.1016/j.scitotenv.2018.02.276.

[61] VDI, VDI 3787. Environmental meteorology. Methods for the human biometeorological evaluation of climate and air quality for urban and regional planning at regional level. Part I: Climate, Blatt 2/ Part 2, (n.d.).

[62] ESI Group, OpenFOAM v1612+, (2016). http://www.openfoam.com/.

[63] S.W. Hong, V. Exadaktylos, I.B. Lee, T. Amon, A. Youssef, T. Norton, D. Berckmans, Validation of an open source CFD code to simulate natural ventilation for agricultural buildings, Comput. Electron. Agric. 138 (2017) 80–91. doi:10.1016/j.compag.2017.03.022.

[64] R. Dadioti, S.J. Rees, Validation of open source CFD applied to building external flows, in: Proc. BS2015, 14th Conf. Int. Build. Perform. Simul. Assoc., Hyderabad, India, 2015.

[65] N.F.M. Kasim, S.A. Zaki, M.S. Mat Ali, A.F. Mohammad, A. Abd Razak, A Verification and Validation Study of CFD Simulation of Wind-Induced Ventilation on Building with Single-Sided Opening, Appl. Mech. Mater. 554 (2014) 696–700. doi:10.4028/www.scientific.net/AMM.554.696.

[66] D.S. Hammond, L. Chapman, J.E. Thornes, Roughness length estimation along road transects using airborne LIDAR data, Meteorol. Appl. 19 (2012) 420–426. doi:10.1002/met.273.

[67] M. Sadeghipour Roudasri, Butterfly plug-in for Grasshopper, (2017). https://github.com/ladybug-tools/butterfly.

[68] J. Franke, M. Sturm, C. Kalmbach, Validation of OpenFOAM 1.6.x with the German VDI guideline for obstacle resolving micro-scale models, J. Wind Eng. Ind. Aerodyn. 104–106 (2012) 350–359. doi:10.1016/j.jweia.2012.02.021.

[69] European Commission Joint Research Center, PV - Gis, (2012). http://re.jrc.ec.europa.eu/pvgis/apps4/pvest.php# (accessed July 20, 2017).

[70] Y.C. Chen, T.P. Lin, A. Matzarakis, Comparison of mean radiant temperature from field experiment and modelling: a case study in Freiburg, Germany, Theor. Appl. Climatol. 118 (2014) 535–551. doi:10.1007/s00704-013-1081-z.

[71] Á. Gulyás, J. Unger, A. Matzarakis, Assessment of the microclimatic and human comfort conditions in a complex urban environment: Modelling and measurements, Build. Environ. 41 (2006) 1713–1722. doi:10.1016/j.buildenv.2005.07.001.

[72] M. Noro, R. Lazzarin, Urban heat island in Padua, Italy: Simulation analysis and mitigation strategies, Urban Clim. 14 (2015) 187–196. doi:10.1016/j.uclim.2015.04.004.

[73] H. Mayer, Urban bioclimatology, Experientia. 49 (1993) 957–963. doi:10.1007/BF02125642.

[74] M. Santamouris, Energy and Climate in the Urban Built Environment, Taylor & Francis Ltd, London, 2001. doi:doi:10.4324/9781315073774.

[75] M. Mitterboeck, A. Korjenic, Analysis for improving the passive cooling of building's surroundings through the creation of green spaces in the urban built-up area, Energy Build. 148 (2017) 166–181. doi:10.1016/j.enbuild.2017.02.005.

[76] H. Taha, Urban climates and heat islands: albedo, evapotranspiration, and anthropogenic heat, Energy Build. 25 (1997) 99–103. doi:10.1016/S0378-7788(96)00999-1.

[77] E. Alexandri, P. Jones, Temperature decreases in an urban canyon due to green walls and green roofs in diverse climates, Build. Environ. 43 (2008) 480–493. doi:10.1016/j.buildenv.2006.10.055.

[78] N.H. Wong, A.Y.K. Tan, P.Y. Tan, N.C. Wong, Energy simulation of vertical greenery systems, Energy Build. 41 (2009) 1401–1408. doi:10.1016/j.enbuild.2009.08.010.

[79] K. Perini, M. Ottelé, A.L.A. Fraaij, E.M. Haas, R. Raiteri, Vertical greening systems and the effect on air flow and temperature on the building envelope, Build. Environ. 46 (2011) 2287–2294. doi:10.1016/j.buildenv.2011.05.009.

[80] G. Pérez, J. Coma, I. Martorell, L.F. Cabeza, Vertical Greenery Systems (VGS) for energy saving in buildings: A review, Renew. Sustain. Energy Rev. 39 (2014) 139–165. doi:10.1016/j.rser.2014.07.055.

[81] T. Safikhani, A.M. Abdullah, D.R. Ossen, M. Baharvand, A review of energy characteristic of vertical greenery systems, Renew. Sustain. Energy Rev. 40 (2014) 450–462. doi:10.1016/j.rser.2014.07.166.

[82] I. Susorova, P. Azimi, B. Stephens, The effects of climbing vegetation on the local microclimate, thermal performance, and air infiltration of four building facade orientations, Build. Environ. 76 (2014) 113–124. doi:10.1016/j.buildenv.2014.03.011.

[83] A. Afshari, A new model of urban cooling demand and heat island—application to vertical greenery systems (VGS), Energy Build. (2017). doi:10.1016/j.enbuild.2017.01.008.

[84] G. Gan, Effect of air gap on the performance of building-integrated photovoltaics, Energy. 34 (2009) 913–921. doi:10.1016/j.energy.2009.04.003.

[85] P.A. Mirzaei, J. Carmeliet, Influence of the underneath cavity on buoyant-forced cooling of the integrated photovoltaic panels in building roof: a thermography study, Prog. Photovoltaics Res. Appl. 23 (2015) 19–29. doi:10.1002/pip.2390.

[86] L. Gaillard, C. Ménézo, S. Giroux, H. Pabiou, R. Le-Berre, Experimental study of thermal response of PV modules integrated into naturally-ventilated double skin facades, Energy Procedia. 48 (2014) 1254–1261. doi:10.1016/j.egypro.2014.02.142.

[87] R.A. Agathokleous, S.A. Kalogirou, Double skin facades (DSF) and building integrated photovoltaics (BIPV): A review of configurations and heat transfer characteristics, Renew. Energy. 89 (2016) 743–756.

doi:10.1016/j.renene.2015.12.043.

[88] O. Zogou, H. Stapountzis, Experimental validation of an improved concept of building integrated photovoltaic panels, Renew. Energy. 36 (2011) 3488–3498. doi:10.1016/j.renene.2011.05.034.

[89] Y. Toparlar, B. Blocken, B. Maiheu, G.J.F. van Heijst, A review on the CFD analysis of urban microclimate, Renew. Sustain. Energy Rev. (2016) 1–28. doi:10.1016/j.rser.2017.05.248.

[90] J. Allegrini, V. Dorer, J. Carmeliet, Coupled CFD, radiation and building energy model for studying heat fluxes in an urban environment with generic building configurations, Sustain. Cities Soc. 19 (2015) 385–394. doi:10.1016/j.scs.2015.07.009.

[91] J. Franke, A. Hellsten, H. Schlünzen, B. Carissimo, K.H. Schlünzen, B. Carissimo, H. Schlünzen, The COST 732 Best Practice Guideline for CFD simulation of flows in the urban environment: a summary, Int. J. Environ. Pollut. 44 (2011) 419–427. doi:10.1504/IJEP.2011.038443.

[92] M. Zinzi, G. Fasano, Properties and performance of advanced reflective paints to reduce the cooling loads in buildings and mitigate the heat island effect in urban areas, Int. J. Sustain. Energy. 28 (2009) 123–139. doi:10.1080/14786450802453314.

[93] V.L. Castaldo, V. Coccia, F. Cotana, G. Pignatta, A.L. Pisello, Thermal-energy analysis of natural ‘“cool”’ stone aggregates as passive cooling and global warming mitigation technique, Urban Clim. 14 (2015) 301–314. doi:10.1016/j.uclim.2015.05.006.

[94] H. Akbari, H.D. Matthews, Global cooling updates: Reflective roofs and pavements, Energy Build. 55 (2012) 2–6. doi:10.1016/j.enbuild.2012.02.055.

[95] N. Curry, P. Pillay, Integrating solar energy into an urban small-scale anaerobic digester for improved performance, Renew. Energy. 83 (2015) 280–293. doi:10.1016/j.renene.2015.03.073.

[96] M. Horváth, D. Kassai-Szoó, T. Csoknyai, Solar energy potential of roofs on urban level based on building typology, Energy Build. 111 (2016) 278–289. doi:10.1016/j.enbuild.2015.11.031.

[97] J. Kanters, M. Horvat, M.C. Dubois, Tools and methods used by architects for solar design, Energy Build. 68 (2014) 721–731. doi:10.1016/j.enbuild.2012.05.031.

[98] N. Mohajeri, G. Upadhyay, A. Gudmundsson, D. Assouline, J. Kämpf, J.-L. Scartezzini, Effects of urban compactness on solar energy potential, Renew. Energy. 93 (2016) 469–482. doi:10.1016/j.renene.2016.02.053.

[99] F. Ali-Toudert, H. Mayer, Numerical study on the effects of aspect ratio and orientation of an urban street canyon on outdoor thermal comfort in hot and dry climate, Build. Environ. 41 (2006) 94–108. doi:10.1016/j.buildenv.2005.01.013.

[100] S.C.M. Hui, M.F. Tsang, Climatic data for sustainable building design in Hong Kong, in: Proc. Jt. Symp. 2005 New Challenges Build. Serv., Hong Kong, 2005.